UNIVERSITY OF CALIFORNIA SAN DIEGO

# Novel Human Organoid Impact Device for Application in Investigating Traumatic Brain Injury

A Thesis submitted in partial satisfaction of the requirements
for the degree Master of Science

in

Bioengineering

by

Christopher Khoury

Committee in charge:

Professor Sameer Bhrugu Shah, Chair
Professor Robert Lie-Yuan Sah, Co-Chair
Professor Ester Jihae Kwon

2022

The Thesis of Christopher Khoury is approved, and it is acceptable in quality and form for publication on microfilm and electronically.

University of California San Diego

2022

TABLE OF CONTENTS

LIST OF FIGURES

LIST OF TABLES

ACKNOWLEDGEMENTS

This project would not be possible without a variety of individuals. First and foremost, I would like to acknowledge and thank Dr. Sameer Shah for his continuous support, mentorship, and guidance in developing this project. Through our countless meetings brainstorming, discussing, and working on each milestone of the project, his time proved to be invaluable to me and gave me the confidence to accomplish anything.

Next, I would like to acknowledge and thank Dr. Ester Kwon, Dr. Angels Almenar-Queralt, Julia Kudryashev, and Rebecca Kandell for their critical and constructive feedback on my project, which helped challenge me to improve my work. Additionally, I would like to thank their support through allowing me to use their lab and their help working through parts of my project.

More specifically, I would like to acknowledge and thank Dr. Angels Almenar-Queralt and Rebecca Kandell for their time, support, and experienced skill-set in running a multitude of experiments for my project. Without them, I would not have been able to run the experiments I needed in the time available and with such caution and experience.

Next, I would like to acknowledge and thank my friend Shivani Shukla, who helped proofread and improve parts of this paper, taught me the basics of immunohistology, and helped on a few tests vital to the project.

I would also like to acknowledge and thank my brother Alex Khoury, for his help in developing and understanding the logic and code necessary for the control system of my project.

Lastly, I would like to acknowledge and thank all my friends and family who supported and loved me the whole way so that I could complete this project and achieve my higher education so that I could build a strong platform to success for the rest of my life.

ABSTRACT OF THE THESIS

Novel Human Organoid Impact Device for Application
in Investigating Traumatic Brain Injury

by

Christopher Khoury

Master of Science in Bioengineering

University of California San Diego, 2022

Professor Sameer Bhrugu Shah, Chair
Professor Robert Lie-Yuan Sah, Co-Chair

Traumatic brain injury (TBI) is a common clinical condition in which the brain is subject to a mechanical injury. This results in short- and long-term clinical symptoms and also increases the risk for future neurodegeneration. Previous studies trying to link TBI with its long-term outcomes have only been performed on animal or culture cell models, but very few studies have been performed on 3D human cellular models. These limitations are major barriers for current translation of preclinical science to clinical implementation. Recent studies suggest that 3D brain organoids may be a useful model to study links between TBI and downstream adverse effects. Previous experiments suggest that injuring organoids one at a time through the use of a modified mouse CCI impactor is tedious and creates high variability. In

this thesis study, a novel brain organoid impact device was designed, manufactured, and tested to effectively model TBI in a human system. Through phantom organoid and human organoid testing, the impact device demonstrated a more simple, accurate, and efficient model to injure brain organoids, compared to its predecessors. The device allows for simultaneous injury of multiple organoids, consistent and controlled deformation of organoids, and the ability to vary impact force and velocity, based on gravity and the defined compression of a spring. This study represents a dramatic improvement over previous TBI organoid models, and will enable us to better understand downstream effects TBI towards improve translation between preclinical and clinical models. It is anticipated that this device will support a variety of experiments to evaluate TBI related diagnostics, therapeutics, biomarkers, and mechanisms of disease progression.

# INTRODUCTION

## What is TBI?

### *Basic Pathophysiology*

Traumatic brain injury (TBI) is a complex injury where the brain is damaged due to an external mechanical force, and is distinctly characterized through two phases: primary injury and secondary injury, illustrated in Figure 1.1. Primary injury occurs directly at initial impact the moment the mechanical force is applied. This phase of injury results in the disruption of integrity of the brain cells and structure through mechanical shearing, tearing, and stretching. The extent of damage is dependent on the biomechanics of impact with respect to force, impact velocity, deformation, and/or spatial extent of injury experienced by an individual. Secondary injury occurs in a progressive manner after the initial impact. After initial impact, any number of biological pathways may be persistently disrupted, either primarily due to injury or as a secondary cascade. For example, intracranial pressure may increase, blood vessels in the area may become damaged, and structural elements of cells may break down immediately after injury. In addition, electrical signal transmission may slow, providing an electrophysiological basis for symptoms such as light sensitivity or memory loss. Beyond disruption of individual cellular function ionic dysregulation and the breakdown of the blood-brain barrier (BBB) may more broadly impact the neuroinflammatory response due to leakage and poor compartmentalization of molecules, ions, amino acids, and proteins, thereby contributing to secondary injury. Secondary injury can last from hours to days to months, and can be caused through a single severe injury or accumulated mild injuries. Persistent secondary injury reflects consequences of continual neurochemical, metabolic, and cellular changes, which include (but are not restricted to) ionic homeostasis imbalance, mitochondrial dysfunction, lipid peroxidation, and membrane degradation, all contributing to neuronal cell death. [4, 5, 24, 37]

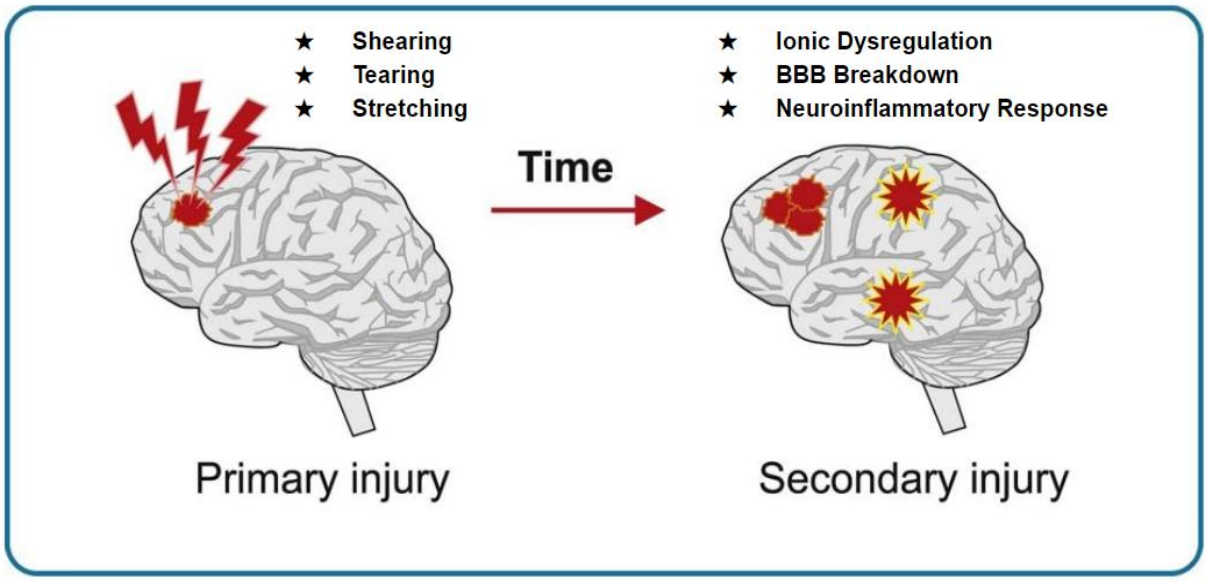


**Figure 1.1:** Concept of primary injury versus secondary injury in TBI. [33]

Damage to brain function reflects damage not only to neurons, the fundamental signaling cells of the CNS, but also glial cells that support neuronal function. In particular, neurons are well-organized by complex networks to communicate via electro-chemical signals. In support of neurons, oligodendrocytes offer structural and functional support by sheathing axons to improve conduction speed of electric signals, which helps nourish axons, regulate signaling, and maintain oxidative reaction balance. Likewise, astrocytes provide structural and functional support to neurons by enveloping synapses, releasing neurotrophic factors, contributing to extracellular ion homeostasis, and regulating the BBB. Microglia play a role in immune defense of the brain and support CNS homeostasis. Of particular note, inflammatory signaling factors alter the phenotype of microglia, allowing their migration to damaged areas of the brain in order to release additional factors or remove harmful material. Each of these cell types are crucial regulatory components within the brain and are thus important to incorporate into in vitro TBI models. [25, 26]

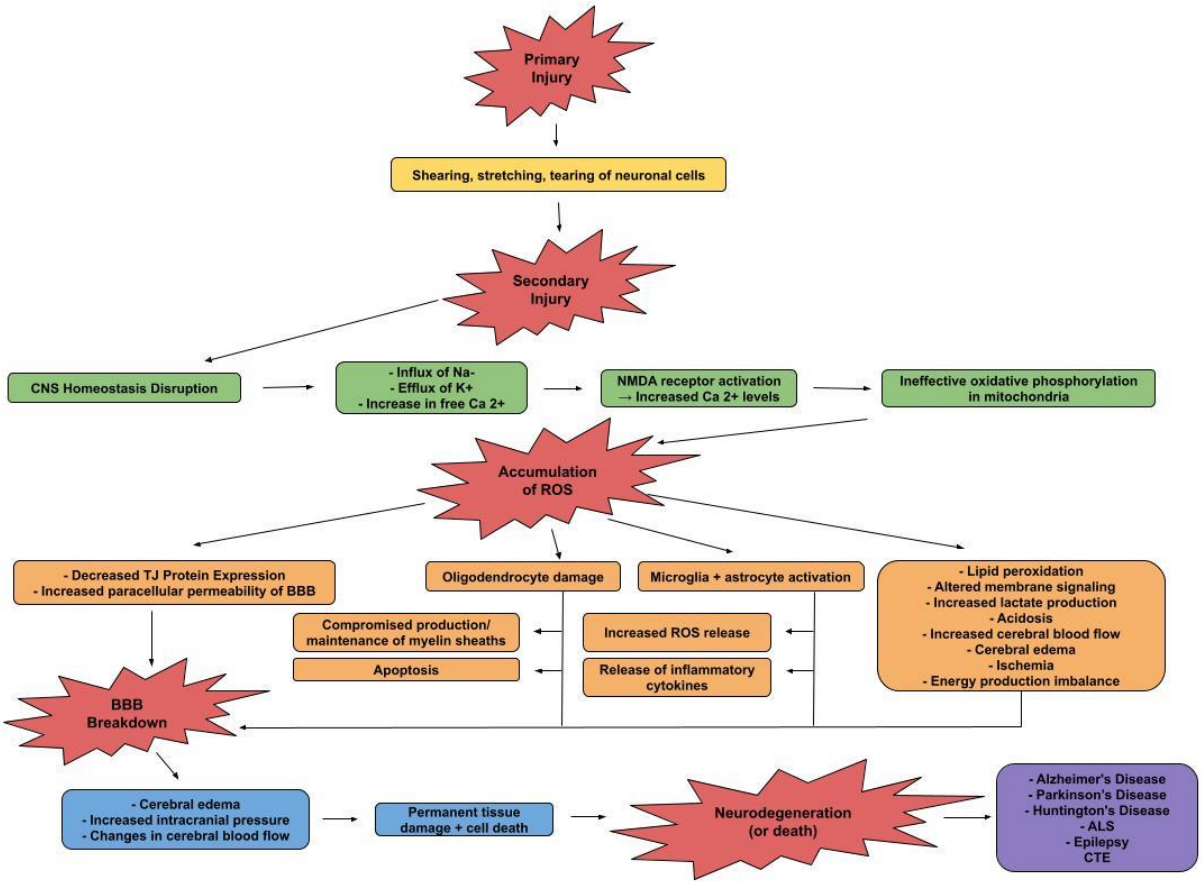


**Figure 1.2:** Cellular and molecular response to TBI.

Figure 1.2 illustrates the complexity of the cellular and molecular response to TBI. As a consequence of direct, rotational, and shear force to the brain, immediate tissue damage and deformation disrupts central nervous system (CNS) homeostasis triggering a multi-cellular response beginning with an unregulated flux of ions. An influx of sodium (Na-) and an efflux of potassium (K+) causes cell membranes to depolarize, releasing excitatory neurotransmitters and further increasing free intracellular calcium (Ca2+). This dysregulation of calcium has many detrimental effects. Increased intracellular calcium (Ca2+) induces glutamate release activating NMDA receptors that further increase calcium levels in both the cytosol and mitochondria, and additionally activates calpain, a protease that degrades cytoskeletal proteins. With increased mitochondrial calcium levels, mitochondrial dysfunction occurs resulting in ineffective oxidative phosphorylation which leads to an accumulation of reactive oxygen

species (ROS). At normal physiological levels, ROS are crucial to neural cell performance. Through neurons and their supporting cells (oligodendrocytes, astrocytes, and microglia), normal ROS facilitates cell communications, CNS homeostasis, inflammatory response, progenitor cell population, long-term potentiation, and synaptic plasticity. In the case of TBI, the brain is susceptible to oxidative stress so when ROS levels are increased there are many repercussions. Within oligodendrocytes, prolonged oxidative stress compromises production and maintenance of axonal myelin sheaths and can induce apoptosis. Microglia and astrocytes further release ROS and inflammatory cytokines increasing damage to an even greater degree. Reactive astrocytes can also cause lasting morphological changes to the tissue and influence gene expression. In addition to increased damage through the neurons supporting cells, ROS contributes to impairing a number of cellular processes, such as lipid peroxidation, altered membrane signaling, increased lactate production, acidosis, increased cerebral blood flow, edema, ischemia, and energy production imbalance. [3, 4, 24, 25, 26]

As ROS continues to accumulate the oxidative stress causes the breakdown of the BBB. The BBB is a critical component in maintaining CNS homeostasis through its semi-permeable barrier that separates circulating blood from the brain environment. It regulates molecules that enter and exit the brain, acting as a blood-brain solute barrier exchange, while also denying peripheral immune cells from entering and removing toxic substances. The BBB consists of specialized endothelial cells called tight junction (TJ) proteins and junction adhesion molecules (JAMs) which regulate paracellular permeability. These endothelial cells are further regulated by their surrounding cells (pericytes, neurons, astrocytes, microglia, etc.) to maintain homeostasis and ionic balance. Following TBI, and furthermore ROS accumulation, TJ protein expression decreases and leads to an increased paracellular permeability of the BBB, which eventually breaks down the BBB. Despite containing microglia, brain-specific immune cells, the loss of TJ proteins allows an influx of additional non-brain-specific immune cells such as neutrophils that worsen the neuroinflammatory response. Larger cells that are usually restricted from entering the brain, such as albumin, also contribute to the dysfunction. Endothelial cell injury, pericyte injury, and astrocyte injury

all result in an increase in BBB permeability promoting further inflammation as well. A significant consequence of this response is cerebral edema due to the excess water accumulation in the brain. Cerebral edema further leads to increased intracranial pressure (ICP) and changes in cerebral blood flow (CBF), which if not immediately regulated can cause permanent tissue damage and cell death, contributing to high death rates seen in severe TBI cases. [4, 5, 24, 26]

*Epidemiology and Diagnosis of TBI*

Current data approximates that annually there are 69 million TBI events worldwide, 1.7 million TBI events in the United States (US), 250,000 TBI-related hospitalizations, and 60,000 TBI-related deaths. It is suggested that more than 1.1% of the US population currently lives with a TBI, accounting for millions of people. [4, 6, 26, 37]

TBI can be caused by traffic accidents, accidental falls, gunshot wounds, explosive blast waves, combat-related events, and collision sports. Collision sports, such as American football and soccer, are reported to have the highest incidence of TBI, and about 10-15% of sports-related injuries are TBI-related injuries. In general, male cases account for more than 73% of all reported TBI events, are 2 times more likely to be hospitalized, and 3 times more likely to die. Older individuals (>75 years) have the highest rate of TBI-related hospitalization of about 32%, and accounts for approximately 28% of TBI-related deaths, equal between men and women. Additionally, and more importantly, TBI is the leading cause of death and disability worldwide among individuals under the age of 45 years, and is an epigenetic risk factor that can cause neurological diseases such as dementia, Alzheimer's disease, Parkinson's disease, and depression. [4, 6, 14, 26, 37]

TBI is heterogeneous, ranging in severity from mild to severe (or even fatal). Severity is classified through the persistence and severity of symptoms, including the common use of the Glasgow Coma Scale (GCS) which clinically scores the injury based on level of consciousness on a scale from 1-15. The GCS measures factors such as eye opening, verbal responses, and motor responses. A score

between 13-15 diagnoses patients with mild TBI (mTBI), a score between 9-12 diagnoses patients with moderate TBI, and a score of 3-8 diagnoses patients with severe TBI. Although the GCS is a useful tool to evaluate TBI severity, it relies on only observable results in the patient highlighting the need for an improved classification system based on biological evidence. [5, 21, 29]

*Risk for Future Neurodegeneration*

As apparent from the above description, the sheer number of cells, cellular processes, and systemic processes affected by TBI, at varying time scales and different degrees of reversibility, have tremendous implications for understanding mechanisms for a particular severity of TBI as well as for diagnosis and treatment strategies. The potential persistence of primary and secondary outcomes including BBB breakdown and axonal transport defects, makes TBI a significant risk factor for neurological disease and death. In fact, these pathways are common underlying events in dementia and numerous neurodegenerative diseases, such as Alzheimer's disease (AD), Parkinson's disease (PD), Huntington's disease (HD), amyotrophic lateral sclerosis (ALS), epilepsy, and chronic traumatic encephalopathy (CTE). TBI is associated with an increased risk for each of these neurodegenerative diseases. The risk of dementia and AD increases around 1.5 times after a TBI, and 5% of all dementia cases worldwide can be attributed to TBI, even for a single mild TBI. Additionally, behavior in individuals with TBI can change as they may express deficits in attention, cognition, sensory processing, communication, severe depression, anxiety, personality changes, aggression, and social inappropriateness. Overall, neuropathology of post-TBI neurological disease is becoming increasingly more characterized, more work can be done to explain the implications of these consequences. [14, 26]

*Therapeutic Strategies*

General solutions after brain injury should prevent progressive neuronal cell death, reestablish neuroplasticity, reduce inflammation, and improve motor and cognitive recovery. Currently, there are inadequate definitive therapeutic approaches to treat TBI, and no medications or techniques that are able

to promote brain repair or reduce brain damage. This is a consequence of our still incomplete understanding of mechanisms underlying persistent dysfunction, a lack of diagnostics to better understand the post-injury state, and limited windows of intervention, based on re-sealing of the BBB and the noted lack of diagnostic strategies. On the other hand, there are many potential general methods to treat TBI, such as pharmacological interventions, biopharmaceuticals, gene therapies, noninvasive interventions, neuroplastic therapeutics, and the use of biomarkers. [26, 35]

Pharmacological interventions include agents that are anti-inflammatory, cell cycle inhibitors, and cyclic adenosine monophosphate (cAMP) augmentors. These interventions have the potential to lessen the development of secondary injury following TBI. An example such as minocycline, inhibits proinflammatory cytokines and microgliosis which has been shown to be effective in preventing neuronal cell death. Additionally, synthetic peroxisome proliferator-activator (PPAR) agonists, such as fenofibrate, can regulate gene expression by suppressing proinflammatory mediators, reducing inflammation, oxidative stress, and cerebral edema. Cell cycle inhibitors, such as flavopiridol, effects cyclin-dependent kinase (CDK) inhibition which can block cell cycle activation in neurons, astrocytes, and microglia, preventing further development of ROS and neuroinflammation. cAMP, a critical molecule that enhances neuronal growth, can be targeted to induce neuronal sprouting, reorganization of neurons in the cortex, and recovery of motor function. In TBI, cAMP signaling reduces which leads to decreased CREB phosphorylation, and by increasing cAMP levels through agents such as phosphodiesterase (PDE) inhibitors, selective serotonin reuptake inhibitors (SSRIs), or serotonin-dopamine reuptake inhibitors (SDRIs) can have positive effects in recovery post TBI. [26, 35]

Biopharmaceutical interventions include the use of biologics and growth factors such as stem cells, peptide therapy, and gene therapy to help reduce the effects of TBI. Therapy through the use of neuronal and mesenchymal stem cells utilizes their neuroregenerative potential to try to treat TBI. Neuroprotective and neuroregenerative efficacy through the use of growth factors has been tested; for example, vascular endothelial growth factor (VEGF), human fibroblast growth factor 2 (FGF2), and

brain-derived neurotrophic factor (BNDF), all show indirect development of neuronal survival through supporting transplanted stem cells in diseased or injured models. Gene therapy, using viral and nonviral-mediated delivery systems, such as adeno-associated viral (AAV) vectors to regulate genes are being developed for treating TBI. AAVs can target genes to either under-express or over-express said genes in order to counter neurodegenerative effects. Micelle-like nanoparticles designed to contain genetic material, DNA or RNA, are also useful in gene therapy because of their ability to enter the brain intranasally and their low immunogenicity. [26, 35]

Noninvasive interventions include brain stimulation and physical exercise. Transcranial magnetic stimulation (TMS) has proven useful in lessening the damage by inducing positive neuroplastic changes. Additionally, neuroplasticity is key in returning to normal neuronal behavior post-TBI. By re-establishing signal transduction pathways and the modulation of the cytoskeletal dynamics, a cellular response can be generated that promotes neuronal growth and plasticity. Membrane lipid rafts (MLRs), are cell membrane cores that are enriched with sphingolipids, cholesterol, and scaffolding proteins, that organize and regulate TrkB and NMDA receptor signaling pathways, adenylyl cyclase 8 (AC8) activity and cAMP production, cytoskeletal dynamics. In combination with pharmacologic agents, MLRs can promote functional and structural plasticity, remove and replace neuronal growth, and improve motor and cognitive performance after a TBI. [26, 35]

To enable better decision-making as to what, if any, therapeutic is most appropriate, diagnostic strategies need to be improved, both with respect to specificity and feasibility. CNS biomarkers represent pathobiological processes at the cellular and subcellular level that are pivotal to the diagnosis of TBI and subsequent monitoring of the effects of the above therapeutic strategies. Currently, there is a lack of existing and proven CNS biomarkers, but there are many candidates that could progress diagnostic, prognostic, and therapeutic development. [26, 35]

At the moment, there is a critical need to develop a better understanding of the underlying pathophysiological processes that occur in TBI. The need for improved translation from preclinical

models to clinical models that can furthermore produce effective therapeutics must be met. Researchers in general, must gain a greater understanding of molecular and cellular mechanisms contributing to secondary injury, provide a variety of brain injury models to test the application of the above therapeutic strategies, develop knowledge on brain pharmacokinetics, perform additional cellular and animal models of secondary injury to study their effects, and to bridge the gap between novel therapy development and TBI relevant measurements. [26, 35]

## Models for TBI

### *Clinical Models*

A variety of investigations have been done to study TBI and its neurodegenerative effects, but since TBI is considered a heterogeneous disease there is a challenge in producing significant clinical models. Many previous trials were largely not useful towards studying TBI as they would measure treatment effects through the GCS, which only relies on symptomatic and observable behavior. There is difficulty declaring clinical phenotypes to mark specific effects of the treatment given, but one of the ways that clinical trials can combat this is through the use of magnetic resonance imaging (MRI). MRI measurements provide information on brain damage and severity, validate diagnoses, and illustrate overall structural response to the therapy. Although MRI and the GCS are useful, they are not particularly insightful, as TBI is a complex cellular and subcellular disease. Additionally, postmortem human tissue samples can be used to investigate TBI, but are not very useful in a controlled study nor can they be examined longitudinally. [14, 25]

### *Animal Models*

Numerous animal models investigating TBI have been developed to study the specific effects of treatment or therapy given. These models have helped distinguish critical injury mechanisms that cause a mild, moderate, or severe case of TBI. Additionally, these animal models, primarily through genetically engineered rodents, have proven useful in identifying significant molecules and pathways for these injury

mechanisms that can be targeted. Rodents are highly available, are low cost, and are behaviorally and genetically very similar to humans, making them great tools to generate a greater understanding of the pathophysiology of TBI. In addition to rodents, pigs and primates have also been used to research TBI. The most common animal models used to study TBI are the controlled cortical impact (CCI) model, the fluid percussion injury (FPI) model, and the weight drop/impact acceleration (I/A) model. [9, 17, 18, 21, 26, 36]

The CCI model induces a precise impact through the use of a striking rod at any angle to the brain. This model is highly reproducible, but has a high mortality rate, and may not simulate the broad-spectrum damage experienced when the entire brain rotates within the skull. Rapid deformation of the brain may sometimes result in focal injury but can also generate cortical tissue damage, subdural hematomas, diffuse axonal injury, and the disruption of the BBB. The diameter of the rod, the depth of impact, the velocity of the rod, and shaped tips to the end of the rod can be varied to influence severity of tissue injury. In contrast, the FPI model induces diffuse injuries to the brain through the sharp increase of intracranial pressure surrounding the brain. Generally, TBI models use a pendulum striking a tube of saline that creates a short fluid pressure impulse delivered to the brain. This model is also highly reproducible and has a high mortality rate. The rapid increase of pressure can lead to the disruption of the BBB, diffuse axonal injury, and an overall neuroinflammatory response. The pressure generated in the brain can be adjusted by changing the height of the pendulum to strike the saline tube. Lastly, the I/A model induces either a mostly focal or mostly diffuse injury by dropping a weight at a specific distance onto a brain or skull. The severity of injury can be altered through changing the weight or height of the drop. The injury produced from this model also leads to cortical tissue damage, diffuse axonal injury, and the disruption of the BBB. An example of this model includes the use of a 450-gram brass weight falling from varying distances (1, 1.5, 2 m) onto animal brains. [9, 17, 18, 21, 26, 36]

Through the use of each of these TBI animal models a variety of measurements can be made including, but not limited to, astrocyte activation, microglia activation, cytokine levels, chemokine levels, and oxidative stress markers. [9, 17, 18, 21, 26, 36]

*Biomechanical Models*

A key to better understanding TBI is to better understand the relationship between biomechanical forces and neuropathy. Through quantitative immunohistochemistry injuries can be investigated and compared to the biomechanical parameters to achieve this understanding. Variables such as velocity, deformation depth, force, and contact duration provide the parameters necessary to monitor mechanical properties seen in damaged brain tissue. Velocity varies amongst all impact models depending on the severity of injury wanted. There is no definitive scale to generate specific severity but the following scale summarizes the general findings amongst the few biomechanical impact models. For more mild injuries, repetitive impacts of speeds between than 0.5 m/s and 2.5 m/s can be used. For moderate injuries, speeds between 2.5 m/s and 4 m/s can be used. For moderate-severe injuries, higher speeds between 4 m/s and 6 m/s can be used. For severe injuries or closed head impacts greater than 6 m/s can be used. Force relates directly to velocity, but not enough information has been found on deformation depth and contact duration. [8, 11, 17, 18, 28, 36]

General biomechanical response for impacts on tissue could follow the Kelvin-Voigt viscoelastic model. This model states that an instantaneous drop in velocity will result in an instantaneous drop in stress. Appendix 1 provides a schematic of this viscoelastic model based on arrangements of spring and dashpot elements. The spring produces instantaneous deformation proportional to load and the dashpot produces aa velocity proportional to the load at any instant. By relating velocity, deformation, and contact duration of a biomechanical impact model to a Kelvin-Voigt viscoelastic model, tissue responses to different compressive loads and strain rates could be accounted for. Although useful, these viscoelastic models were not considered for the following thesis. [13, 38]

*In-Vitro Models*

In-vitro models of TBI involve growing neurons in a 2- or 3-dimensional matrix and applying tensile, shear, or compressive forces to whole cells or individual cell compartments. In comparison to animal models, in-vitro models can reduce complexity as there is greater control over the experimental conditions, it is easier to measure cellular responses immediately, but they do not replicate the complexity of an entire brain. It has been found that about two-thirds of TBI in-vitro experiments apply their load through uniaxial stretch. A stretch injury is induced by growing neurons on elastic silicone membranes that are stretched via a rapid pressure pulse. To influence mild, moderate, and severe injuries in the cells, the rate and magnitude of the load can be varied to produce such effects. Other major load application methods included blast, compression, scratch, and shear. Key processes that have been studied through the use of in-vitro models include membrane disruptions leading to ionic dysregulation, inflammation, microtubule and axon damage, and cell death. Generally, rodent cell origin accounted for about 84% of the species types tested, while about 15% of the in-vitro studies used human cells. Although using animal cell in-vitro models has been key to current TBI pathophysiology understanding, therapeutic targets identified have not effectively translated to clinical trials. Greater use of human cells requires more attention to bridge this gap to clinical trials. 3D models can also be used to represent more thorough loading conditions and consequences, which can provide a more realistic injury response. Through a variety of cell types, such as astrocytes, hippocampus cells, neurons, oligodendrocytes, endothelial cells, vascular smooth muscle cells, neuroblastomas, microglia, and pheochromocytomas, a collection of injury responses can be monitored. These injury responses include axonal injury, calcium activity, cell death, inflammation, long-term potentiation deficits, and ROS. In general, in-vitro models have been pivotal towards our understanding of TBI, and allow follow-up of key findings in vivo, but more work can be done. Future models need to have a greater diversification of load application that will more closely mimic in-vivo brain impacts, there needs to be greater use of human brain cells as animal cells do not completely translate to clinical trials, and more comprehensive set-ups that can model the structural

complexity of the brain including brain cells so that more effective TBI therapeutic targets can be discovered. [18, 36]

*Organoid Models*

Human stem cell derived brain organoids are a great resource that combines 3D cellular models and human cell models. Generated through hiPSC (human induced pluripotent stem cells) derived engineered tissues, organoids provide a step towards being able to translate in-vitro models to clinical trials. There are only a few studies that investigated oxidative-stress induced TBI responses in brain organoids and how these injury mechanisms relate to CNS neurodegenerative diseases. Multicellular 3D human organoids containing endothelial cells, pericytes, astrocytes, microglia, oligodendrocytes and neurons have been used to evaluate the effects of hypoxia and neuroinflammation on BBB function previously. Additional studies investigate protein disruption, altered differentiation, and cell death during hypoxia treatment. These studies have demonstrated the utility of organoids in regards to the effects of oxidative stress on brain cells and can prove to be useful for a more comprehensive investigation into the pathophysiology of TBI, diagnostics, and therapeutic effects. Despite this, there are not many studies inducing the mechanical deformation of organoids to model TBI. The main purpose of this paper is to investigate TBI through the use of brain organoids in combination with a novel impact device that mechanically deforms the organoids. Organoids will be explored more in depth in the next section. In summary of the general models used for TBI, Table 1.1, a comprehensive pros and cons are compared. [19, 26]

**Table 1.1:** TBI Model Advantages and Limitations [9, 8, 11, 17, 18, 19, 20, 25, 26, 28, 36, 37]

| Model Type | Advantages | Limitations |
|---|---|---|
| 2D Culture | • Derivable and generated from patient iPSC or ESC<br>• Readily available, easily manipulated, low cost<br>• Highly scalable and high throughput<br>• Abundant culture methods and analytical techniques<br>• Widely used to study CNS disease progression<br>• Can model near-physiological morphological changes and responses to oxidative stress<br>• Can obtain functional cell and tissue specific information | • Lacks 3D brain structure and microenvironment<br>• Limited complexity in tissue composition and cell state<br>• Poor representation of the in vivo physiological environment<br>• Lack of relevant data on cell–extracellular matrix or cell–scaffold interactions<br>• Limited differentiation capacity |
| Animal | • Intact 3D brain structure<br>• Comparable size and anatomical structure<br>• Can monitor the behavior of specific cell types and disease progression<br>• Can obtain useful measures of altered cognitive and behavioral states<br>• Can obtain functional whole body 3D information, i.e., systemic responses | • Do not always translate to humans due to inter-species differences<br>• Significant metabolic, anatomical, and physiological differences to humans<br>• Low throughput<br>• Differences in brain mass, development, cellular organization, and regionalization |
| Postmortem Human Tissue | • Intact 3D brain structure and microenvironment of human origin<br>• Accurate size and anatomical structure<br>• Specific cortical cell types and precise developmental cues<br>• Visible tissue degeneration in specific brain regions<br>• Can obtain patient specific measures of disease states<br>• Can identify terminal pathological features of disease states across diverse human populations | • Limited availability and low throughput<br>• Difficulties in genetic manipulation<br>• Loss of data on altered cell function and behavior due to tissue degeneration during processing<br>• Decreasing donor/ sample availability<br>• Ethical and practical limitations of investigating live/ dead human brain tissue<br>• Poor study control to determine if observations/results are due to disease or caused by other agents |

**Table 1.1:** TBI Model Advantages and Limitations (cont.) [9, 8, 11, 17, 18, 19, 20, 25, 26, 28, 36, 37]

| Model Type | Advantages | Limitations |
|---|---|---|
| Organoids (3D Culture) | • Intact 3D brain structure and microenvironment<br>• Derivable and generated from patient iPSC or ESC<br>• Highly scalable and high throughput<br>• Capacity for self-organization and differentiations<br>• Can obtain organ-specific 3D information | • Process is labor intensive, time consuming, expensive, and technically limited<br>• No definite standards or parameter to generate and culture brain organoids<br>• Limited maturity and size<br>• Relies on growth factors and differentiation protocols<br>• Variability among batches and studies |

**Organoids**

As introduced earlier, current organoid technology includes the generation of a 3D tissue derived from hiPSC. These organoids are developed in vitro by arranging multiple cell types together in a tissue culture to closely resemble the organ of interest. When these cell types are supplemented with specific promoters the development of the organoid is pushed in a certain trajectory to function as their intended organ. Through self-assembly, self-patterning, and self-driven morphogenesis, the organoid emerges. When the organoids have fully developed and grown, they can serve as complex functional surrogates that have similar mechanics at the molecular, cellular, tissue, and organ level. Through advancements in stem cell biology over the last couple decades, organoid research has evolved substantially, but with continual improvement, organoids could be developed in large variable quantities that allows researchers to establish thoroughly reproducible, scalable, and high-throughput translational models. [7, 25]

*Brain Organoids*

Brain organoids are three-dimensional neural tissues derived from the self-organization of hiPSC. These brain organoids resemble the organization, developmental timing, and transcriptional epigenetic signature of a primitive human fetal brain. There are two types of brain organoids: patterned or non-patterned. Patterned brain organoids call for a specific set of growth factors to guide the cells

development towards specific brain regions, whereas non-patterned brain organoids allow for different brain regions to develop into a single unit. For example, through the manipulation of TGFb and BMP pathways and GSK-3, forebrain organoids could be developed. Midbrain organoids can be generated through manipulating SHH and FGF growth factors, as well as WNT-3A and SHH for hypothalamus development. Additionally, human brain organoids can be genetically edited via genome editing technology such as CRISPR and TALEN. Through the various developmental methods to format these brain organoids towards specific characteristic features and various disease states, brain organoids are currently a novel and innovative model to study human neurodevelopment, neurological disorders in the CNS, and neural response to oxidative stress caused by TBI. [7, 26, 34]

These brain organoids differ from rodent brains and human brains mainly in size, complexity, and maturity. The brain organoids used in the following experiments are approximately found to have a diameter of 1.25 mm, whereas rodent brains and human may have an approximate diameter of 28 mm and 560, respectively, based on overall surface area. In terms of complexity, the brain organoid is a miniscule model of a rodent or human brain that can represent small regions or types of the brain based on the certain growth factors provided, but it is not a functional brain. Human brains have an approximate of 1000 times as many neurons as rodent brains, which may illustrate the stark difference in neuronal structure between functional brains and brain organoids. Similarly, since the neuronal structure is much less complex, human organoids are much less mature than rodent and human brains. Human organoids are typically grown over a course of 6 months from initial cell derivation until they reach their full maturation, whereas rodent brains are found to reach full adult maturation at a post-natal date greater than 3 months, and human brains reach full adult maturation after 20 years. A future literature review or study would be beneficial in identifying key differences between brain organoids, rodent brains, and human brains. [10, 16, 27]

*Advantages and Limitations of Brain Organoids*

Brain organoids are valuable tools to study CNS development, disease and tissue repair. There are many advantages for the use of brain organoids, along with limitations as well. One of the significant advantages of brain organoids is their physiological relevance, reproducibility, and ability to generate patient and disease specific models without ethical or practical limitations of investigating live human brain tissue. Brain organoid cultures resemble in vivo conditions much closer than 2-D, planar cultures, which allows for greater investigation into cell interaction, differentiation, and communication. These culture conditions allow for the complete containment of a neural microenvironment that includes neuronal progenitors, mature neurons, astrocytes, and oligodendrocytes. Additionally, brain organoids can be maintained for extensive periods of time, which allows researchers to accurately model disease progression. Brain organoids also have demonstrated potential in modeling oxidative stress as pharmacological and genetic tools are able to induce OS in brain organoids, patient-derived brain organoids are able to demonstrate disease specific effects to OS, and functional and anatomical features of development and disease influenced by ROS and neuroinflammation are able to be captured. [7, 19, 26, 34]

The most significant limitation of brain organoids, however, is that the process of generating these brain organoid cultures from patient derived cells is labor intensive, time consuming, costly, and technically limited, which is challenging in demonstrating consistency in each batch and study. Consistency among the scientific field is also difficult as there are no definite standards or set parameters in brain organoid culturing methods and classes. The size of the brain organoid is also an issue as since they are only a few millimeters long, the health and long-term maintenance of the cells within the organoid is limited. Additionally, since brain tissue is intrinsically complex, only specific regions, functions, or features through specific growth factors and differentiation protocols can be modeled. With this in mind, although brain organoids can resemble the organization and complexity of the brain, it can never be stated that brain organoids fully replicate the development, morphology, molecular patterning, or

disease phenotypes of the brain. In Table 1.2 below, these advantages and limitations are summarized. [7, 19, 26, 34]

**Table 1.2:** Brain Organoid Advantages and Limitations [7, 19, 26, 34]

| Advantages | Limitations |
|---|---|
| • Physiologically relevant<br>• Highly reproducible<br>• Ethical and practical<br>• Derivable from patient-iPSC<br>• Brain-like 3D microenvironment<br>• Can be used to model human disease progression<br>• Ability to for self-organize and differentiate<br>• Highly scalable and high-throughput<br>• Demonstrate potential in modeling oxidative stress | • Process is labor intensive and time consuming<br>• Expensive<br>• Technically limited<br>• No definite standards or parameter to generate and culture brain organoids<br>• Limited maturity and size<br>• Relies on growth factors and differentiation protocols<br>• Variability among batches and studies<br>• Cannot fully and completely replicate the complexity of the human brain |

*Applications of Brain Organoids*

Brain organoids present a useful tool in drug screening, and more specifically, for a greater understanding of the multicellular implications of TBI and neuroinflammation. One of the most distinctive examples in current research using brain organoids was to establish a causation between the Zika virus and microcephaly cases in Brazil, a condition where a baby's head is significantly smaller than expected, often due to abnormal brain development. Exposing hiPSC-derived brain organoids to an isolated Brazilian Zika virus strain, it was shown that the virus was attracted to neural progenitor cells, which are key in the development of the brain. Successful drugs, such as chloroquine and sofosbuvir, led to the protection and treatment of Zika-virus infected human organoids. Another example in current research using brain organoids was to model the effects of hypoxia and neuroinflammation on BBB functions. Human brain organoids consisting of human brain microvascular endothelial cells, pericytes, astrocytes, microglia, oligodendrocytes and neurons, were cultured in a hypoxic chamber for 24 hours and showed increase permeability, proinflammatory cytokine production, and increase oxidative stress.

Through the use of anti-inflammatory agents affecting the endocannabinoid system, inflammatory cytokine levels, ROS, and inflammation in the hypoxic organoids are reduced. Although brain organoid models are relatively new, there have been a number of significant brain organoid models in the scientific community, exploring applications that allow for a greater understanding of major neurodegenerative disorders such as AD, PD, brain cancer, TBI, stroke, BBB disruption, and others. In the review by Tan, et. al., the major achievements of human brain organoid models are summarized including the specific target of the models, their achievements, the physiological and pathological model, and references for further exploration into these applications. [19, 23, 25, 30, 34]

## Current Organoid Injury Models

### *3D Printed Organoid Impactor*

Despite the numerous brain organoid applications, as well as the substantial TBI animal or in-vitro impact models, there are not many studies that combine TBI impact models and brain organoids. In a study done by Wen Shi, et. al., an in-vitro mild TBI modeling system was designed and evaluated using a 3D printed mini-impact device on 3D cultured human iPSC derived neural progenitor cells. Shi calls for a more human relevant model to bridge the gap between preclinical studies and clinical treatments as treatment strategies developed from animal models have failed in translating to TBI patients. Through the improvement of hiPSC technology and a 3D printer, Shi fabricated an impact device capable of convenient, reproducible, and repeated weight drop impact injury to human brain organoids. In this study, it was demonstrated that single mild impacts induce minimal injury with easy recovery, but repetitive mild impacts lead to neuron loss, reactive astrogliosis, and glial scar formation.

The mini-impact device consisted of a 3D printed neurosphere (brain organoid) impactor, guide construct, and neurosphere holder. The device was designed for the guide construct to allow for a controlled free fall of the impactor onto the holder. The holder is able to slide in and out, and holds a single 0.5 mm organoid that fits within a 3 mm wide and 0.25 mm deep semi-sphere. The impactor had a

mass of 0.9 g, and was dropped from either 15 mm or 30 mm in height, considered as half-impact or one impact, respectively.

A finite element model simulation using Abaqus software illustrated the distribution of minimum principal strain in the brain organoid at the maximum indent depth, and the impact induced strain for a half impact, one impact, two impacts, and ten impacts. As expected, they found that the equivalent plastic strain (PEEQ) increased as the quantity of impacts increased, corresponding to accumulated cell damage after multiple impacts.

Following the simulation, a single impact experiment was run to explore whether or not a single mTBI affected proliferation and differentiation of the brain organoids. Compared to the control, half impact and one impact showed an increase in axonal outgrowth damage, along with a significant lactate dehydrogenase (LDH) release directly after impact signifying neuronal damage. Immunofluorescent (IF) staining of caspase-3, a protease activated upon apoptotic cell death receptor signaling, demonstrated an increase on day 7 after injury, confirming significant apoptosis. The control, shown by Ki-67 staining, showed no significant difference; NeuN and GFAP staining, the long term (day 27) neuronal maturation and astrocyte activation stains, respectively, also showed no significant difference. Through this experiment it might signify that a mTBI was indeed induced, while the threshold for long term damage, characterized by astrocyte activation, seen in TBI was not met.

Next, repetitive mTBI via multiple mild impacts at a 72-hr interval every two impacts were induced. IF staining of NeuN and GFAP on day 27 after initial impact, showed a significant decrease of NeuN protein indicating a decrease in mature neurons, and a significant increase in GFAP protein indicating astrocyte activation. Additionally, the upregulation of GFAP revealed the formation of a glial scar that is similar to those found in TBI patients. Characteristic pathology of repetitive mTBI was produced and mimicked through the use of this model, as seen through neuron loss, reactive astrogliosis, and a glial scar.

Another experiment performed was to incorporate and measure human microglia clone 3 (HMC3) into the model to monitor TBI progression. The microglia were introduced into the surrounding area of the organoid and directly after the first impact in this two-impact specific experiment. IF staining showed migration and infiltration of the microglia into the damaged organoid, along with additional axonal damage. This migration was further confirmed by ionized calcium-binding adapter molecule 1 (Iba-1), which was stained and present in the peripheral regions of the damaged organoids, but not in the control. IF staining of this same experiment confirmed significant neuronal cell death marking Caspase-3, no significant difference in Ki-67 staining, significant decrease in NeuN positive cells, and significant increase in GFAP expression. Lastly, a cytokine array assay was performed to differentiate the pro-inflammatory species present in the groups without microglia versus the groups with microglia.

Overall, this study revealed that the brain organoids develop reactive astrogliosis and glial scar formation after repetitive mild impacts, whereas after one or two mild impacts there is no astrocyte activation. It is also clear of the biological relevance and potential for human brain organoids in TBI impact studies as the model mimics typical brain impact injury pathology. [28]

*CCI Organoid Impactor*

In a study done by Yung Chia Chen, et. al., a modified CCI device was used to model mTBI mechanics in mice. Their device has similar features of a typical CCI such as an impactor striking and returning to the original positions, but is modified by the use of a rounded silicone tip and modifying impact speed to loading forces seen in mTBI. The impactor moved 2.1mm at 0.43 m/s of the exposed surface of the mouse brain. This study focused on very slow speeds to ensure a mTBI, whereas they express that higher impact speeds such as 4-6 m/s could be achieved for more damaging injuries. [8]

At the University of California, San Diego (UCSD), the Kwon Lab is employing the modified version of the modified CCI device above onto brain organoids in order to create tools, diagnostics, and therapeutics for the CNS. At the moment their goal is to measure calpain-1 activity in injured organoids

with a TBI-ABN targeted to hyaluronic acid (HA). Organoids of approximately 1.5mm in diameter were impacted using their modified CCI device with a 1mm diameter probe, at 2 m/s, and at a depth of 0.5mm. Although there was promise in these experiments, the modified CCI device proved inefficient in production of the injured brain organoids, as only one organoid could be injured at a time with hours of set up for the single organoid. In assistance of the Kwon Lab, the Shah Lab at UCSD has taken on the project to design and manufacture a novel brain organoid impactor device that will provide the Kwon Lab and other labs the equipment they need to variably injure brain organoids efficiently. To provide context to developing design criteria for such a novel brain organoid impactor, Table 1.3 lists out the advantages and limitations of the 3D printed organoid impactor and the modified CCI organoid impactor.

**Table 1.3:** Advantages and Limitations of Current Organoid Injury Models [8, 28]

| Organoid Injury Model | Advantages | Limitations |
|---|---|---|
| 3D Printed Organoid Impactor | • Simple weight drop model with easy set up<br>• Reproducible<br>• Great for mTBI experiments | • No variability in speed, depth of drop, and depth deformation<br>• No variability per experiment<br>• Only great for mTBI experiments, not severe TBI<br>• Can only injure one brain organoid at a time |
| Modified CCI Organoid Impactor | • Reproducible<br>• Controlled deformation of the tissue<br>• Precise velocity control | • Complex and large pneumatic system<br>• Requires technical training and a lengthy set-up process<br>• Inefficient production of injured brain organoids (can only injure one brain organoid at a time)<br>• No variability per experiment |

## Clinical Relevance for TBI Brain Organoid Models

### *Physiological Relevance*

Brain organoid models have a significant potential to effectively understand mechanisms of TBI, their risk for future neurodegeneration and disease, allows for the ability to screen drugs and therapeutic methods, and measure biomarkers that are relevant to animal and clinical models. It has been suggested that the functional and structural resemblance follows the same allometric scaling rules of organoids and mammalian organs. When assessing the potential of organoids to be physiologically relevant in vitro models to animal or clinical models, it has been found that physiologically relevant organoids should obey allometric scaling laws, such as obeying Kleiber's law, which states that the basal metabolic rate of an organism scales with its body mass to a universal power law, and that the oxygen levels to the organoids core must be greater than critical threshold. In addition, when utilizing a brain organoid impact model, correlation between severity of the impact and the magnitude of effect must be determined. As seen in the 3D printed organoid impactor model, through the variation of impact height and impact quantity a standard response was induced. When impacted a mild single time minimal damage was done with no long-term effects, whereas impact multiple mild times induced a pathophysiological response characteristic of mTBI. There is no current standard scale to correlate the severity of the impact with the magnitude of effect, but there is a foundation to further determine the correlation in the following study. [20]

### *Genetic Relevance*

Another consideration when assessing organoid's ability to translate and understand the mechanisms of TBI is the genetic variability in the differentiation of organoids. Since the organoids in question are derived from humans, they can either be manipulated genetically or represent the variability of the human genome. In a study evaluating genetic variability in differentiating human kidney organoids, it was found that there was significant variation between experimental batches, while the individual

organoids within the batch showed minimal variation. It is also noted that as the model becomes increasingly more cellularly complex, the greater the variation. Normalization of the specific genes that are most variable between the batches is possible, however it risks removing relevant phenotypic information. Through selecting for specific cell types within the organoid, technical variation can be reduced. In addition, the genetics of the organoid can be modified through a multitude of techniques. Transient techniques, such as adeno-associated virus (AAV) and electroporation, can be used to allow protein expression or the production of short interfering RNAs (siRNAs) for a short period of time. Stable genetic modifications, such as use of lentiviruses, transposon-like systems, and CRISPR/Cas9, can be used to introduce genetic modifications and pass this information on to future cell generations. When deciding between each of the different types of genetic modification techniques it is important to address the nature of the genetic modification, the organoid development stage at the time of genetic modification, and the target cells of the genetic modification. In addition, a combination of transient and stable genetic modification techniques show promise for studying brain organoid development and ability to counteract the risk of losing phenotypic information in an attempt to normalize genomic variation. [12]

*Drug Screening and Biomarkers*

Through building physiological relevance and understanding how to manipulate and control genetic variability, the potential for brain organoid models in understanding the mechanisms of neural disease, not just TBI, becomes clear. These models have the ability to effectively screen drugs before injury, right after injury, or long term after injury. In addition, there is potential to discover or confirm specific biomarkers that are particularly relevant in linking mechanisms of TBI and neurodegeneration, which could play a significant role in identifying, diagnosing, and treating TBI. According to the FDA, the types of biomarkers that exist include molecular, radiographic, histologic, and physiologic. Molecular biomarkers allow you to measure biophysical properties through biological samples, such as plasma, serum, cerebrospinal fluid, biopsies, etc. Radiographic biomarkers provide information that can be measured through imaging studies. Histologic biomarkers characterize biochemical or molecular changes

in cells, tissues, or fluids. Physiologic biomarkers measure the general physiological processes. Biomarkers have applications involving screening, susceptibility or risk, diagnostics, prognostics, monitoring, and safety. [1, 14, 15, 22, 24, 31, 32]

To reflect the pathophysiological processes that occur in a TBI, CSF and blood biomarkers are most effective in marking the effects of TBI on the CNS. In Table 1.4 below, a detailed list of specific biomarkers that have the greatest potential and relevance for use in researching TBI is provided.

Although these biomarkers show potential by predicting severity of injury and clinical outcomes, there are limitations. Some of the biomarkers listed are not CNS specific and do not completely reflect specific metabolic changes, vascular pathologies, and inflammation during secondary injury that is responsible for progressive neuronal damage post-TBI. In order to improve TBI therapeutic interventions, biomarkers that identify these specific pathophysiological processes must be determined. There is no current convincing biomarker that is evident in accessing TBI and detecting neurodegeneration effectively.

**Table 1.4:** Potential TBI Biomarkers [1, 14, 15, 22, 24, 31, 32]

| Biomarker | Description | Application | Cell Target |
|---|---|---|---|
| NF-H,L | Neurofilament heavy chain, Neurofilament light chain | Predictor of injury severity, track disease progression | Neuron |
| GFAP | Intermediate filament protein of the astrocytic cytoskeleton | Differentiation of injury severity | Astrocyte |
| UCH-L1 | Neuron-specific cytoplasmic enzyme involved in protein ubiquitination and elimination via the ATP-dependent proteasome pathway | Differentiation of injury severity | Neuron |
| NSE | Neuron-specific glycolytic enzyme that is released into the extracellular space upon neuronal damage and death | Predictor of neuronal damage | Neuron |

**Table 1.4:** Potential TBI Biomarkers (cont.) [1, 14, 15, 22, 24, 31, 32]

| Biomarker | Description | Application | Cell Target |
|---|---|---|---|
| MBP | Small (18.5 kDa), positively charged extrinsic membrane protein that constitutes ~30% of the total protein of the CNS myelin | Predictor of neuronal damage and demyelination | Oligodendrocytes |
| Tau | Microtubule associated protein involved in regulation of microtubule dynamic stability | Predictor of neuronal damage and neuroplasticity | Neuron |
| IL-6,8,10 | Neuroinflammatory cytokine proteins (interleukins) | Predictor of neuroinflammatory response | Neuron |
| SBPD | Fragments of spectrin, a cytoskeleton protein, that is cleaved by calpain and caspase-3 | Predictor of severity of injury | Neuron |
| miRNA-16, 92a, 765 | MicroRNAs that show change in expression within 48hrs of injury | Monitoring of specific miRNAs to relate genetic response with severity of injury | RNA |
| NLRP3 | Protein subunit of the NLRP3 inflammasome that upregulated in response to astrocyte and microglia reactivity | Predictor of neuroinflammatory response | Astrocyte |

**Future Work**

In the following paper, a novel brain organoid impact device was designed and manufactured to induce TBI onto brain organoids. This device has the potential to improve upon past designs, provide variability to experiments, and improve production efficiency of injured brain organoids for investigation. Through this novel organoid injury model, it is expected to provide a platform to better understand the pathophysiology of TBI, identify and discover significant biomarkers of TBI, and effectively screen drugs that translate to clinical models.

# DESIGN RATIONALE & PROTOTYPE FABRICATION

## System Requirements

As seen in Table 1.3, there are advantages to the previous brain organoid impact models, but there are many limitations that must be addressed. In this study, we set out to improve upon those brain organoid impact models and design an elegant, compact, and efficient device for variable direct impact experiments on brain organoids. The system requirements, defined in Table 2.1, drove the iterative design process in creating this novel brain organoid impact device.

**Table 2.1:** System Requirements & Rationale

| System Requirements | Rationale |
|---|---|
| Design must be compact and portable | • The device must fit within a standard lab hood (2')<br>• The device must be transportable between labs for a variety of experiments |
| Design must be easy to manufacture, assemble, and use | • Previous devices required complex parts that was not easily manufacturable<br>• Previous devices required an extensive set up and assembly time<br>• Previous devices required training processes to use<br>• The device must have a short preparation time and be simple for anyone to use |
| Design must be low-cost | • The device parts must cost less than $1000 |
| Design must be sterilizable | • The device will be used in a lab and the material must be able to undergo sterilization protocols such as UV light sterilization |
| Design must allow for efficient experimental use | • Previous devices were only able to produce one injured organoid at a time, with hours of preparation<br>• The device must increase the production output of injured brain organoids for more experimental use |
| Design must allow for variable experimental use | • The device must allow the ability to induce different levels of injury severity<br>• The device must be able to control the force, velocity, and deformation of the organoid<br>• Will allow for variety in brain organoid impact experimental applications<br>• Will allow for control over range of damage on the brain organoids |

**Table 2.1:** System Requirements & Rationale (cont.)

| System Requirements | Rationale |
|---|---|
| Design must allow for variability in the organoid holder | • Organoids are not always produced at the same size<br>• Different sized organoid holders allow for additional variability to experimental applications |

## Final Design

### *Brainstorm*

Beginning with an extensive brainstorm process, multiple iterations of the design were developed, leading to a finalized model. The following model can be described as a gravity and spring-loaded vertical drop assembly. Other proposed designs included utilizing a swinging pendulum to cause impact, a linear actuator similar to the CCI model, and a dart dropper design. The vertical drop assembly was determined to be the best of the proposed designs because it aligned best with the system requirements. Initial brainstorms of the vertical drop assembly included the use of gravity or spring forces to generate the force necessary to induce TBI, vertical rails to accurately guide the impactor, various impact tips, a motor and control system to control the height of the impactor or compress the spring in order to induce a specified amount of force, and various organoid holders for different sized organoids.

### *First Iteration*

The first iteration of this design was made up of an extendable cube frame that utilized linear stages to control the height of the vertical drop. Vertical ball bearing guide rails were designed to oppose each other on each side of the cube, attaching to the impact tip. At the center of the base, a single organoid holder was screwed into the frame, with variable holders designed for different sized organoids or applications. The mechanical assembly consisted of a spring compression mechanism through use of physical compression or motorized compression in combination with gravity. The springs would be

interchangeable to induce different velocities and forces. The idea was for the spring to be compressed either physically or with a motor to propel the impact tip to the center organoid holder.

After review, the overall idea behind the design worked but some things needed to be revised. The organoid holder was now expected to impact multiple organoids at a time (n =15 or greater) for efficient production purposes, along with the need to be easily removable and insertable without screws. A sensor needed to be introduced in order to know when the impactor hits, along with a non-mechanical trigger to release the spring-loaded impactor so that there is minimal variability in the release. Additionally, a mechanism needs to be introduced in order to pop the impactor back up after impact to limit the constant deformation on the organoids, along with an impact stopper through the use of rubber pads or more in order to ensure the impact isn't too great and has minimal vibrations.

*Second Iteration*

In the second iteration, the assembly was completely restructured to reduce material usage and make the assembly look less bulky and more aesthetic. The base of this assembly consisted of a detachable hollow base connected by pins and a large square hole to insert a post. Within the base is the control system, a linear stage, and a linear actuator. The linear stage fits within the hollow base and controls the height of an attachment with rubber pads which further controls the deformation of the organoids. The linear stage was chosen to be small enough to fit within the base and has precise control of height. The linear actuator, which also fits within the hollow base, will work in conjunction with a distance measuring sensor in order to pop the impactor up a few millimeters directly after impact to ensure that there isn't constant deformation on the organoids. The linear actuator also was chosen to be small enough to fit within the base and strong enough to push the impactor back up. On the outside of the base sits the organoid holder, which was designed to hold 186 organoids and includes a push fit insert. The holder also has a square cut in the center to allow for the linear stage attachment and linear actuator to fit through to act on the impactor. The holder was arbitrarily chosen at the time to space the holes by 6mm and ran across the entire plate.

Conversely, the top portion of the assembly consists of a spring assembly that pushes an impact plate down a single guide rail attached to a post that leads down to the base. The post has holes that line up with the guide rail and has a t-shaped insert on the sides in order to slide in the top assembly housing. Within the housing consists of the impact plate which is attached to an l-bracket which then attaches to the guide rail. Additionally, the impact plate has a circular slot which fits the spring that will induce the force, so that there is no buckling or sliding of the spring. Embedded into the housing sits a magnetic switch, made by MagSwitch, that will ensure a consistent and quick release speed of the impact mechanism. The spring assembly consists of a plastic knob, a threaded rod, the spring, and a spring cap. The rod is embedded in the housing and can be twisted via the knob to decrease the height of the spring into the magnetically fixed impact plate on the other side, resulting in compression of the spring.

In order to specify dimensionality of the device to generate the force needed, a force-velocity analysis using MATLAB was performed. By calculating the hypothetical mass of the impactor and height of the drop based on design, and varying the spring constant and compression of the spring, force and velocity curves were generated. The range of velocity that is targeted is between 4 m/s and 10 m/s, which will induce severe TBI on the brain organoid based on previous models. Through the use of this MATLAB code, force-velocity relationships, seen in Figure 2.1, were generated to further understand and predict the implications of different spring constants, spring compression, drop height, and mass of the impactor. Appendix 2 provides the MATLAB code used for such calculations.

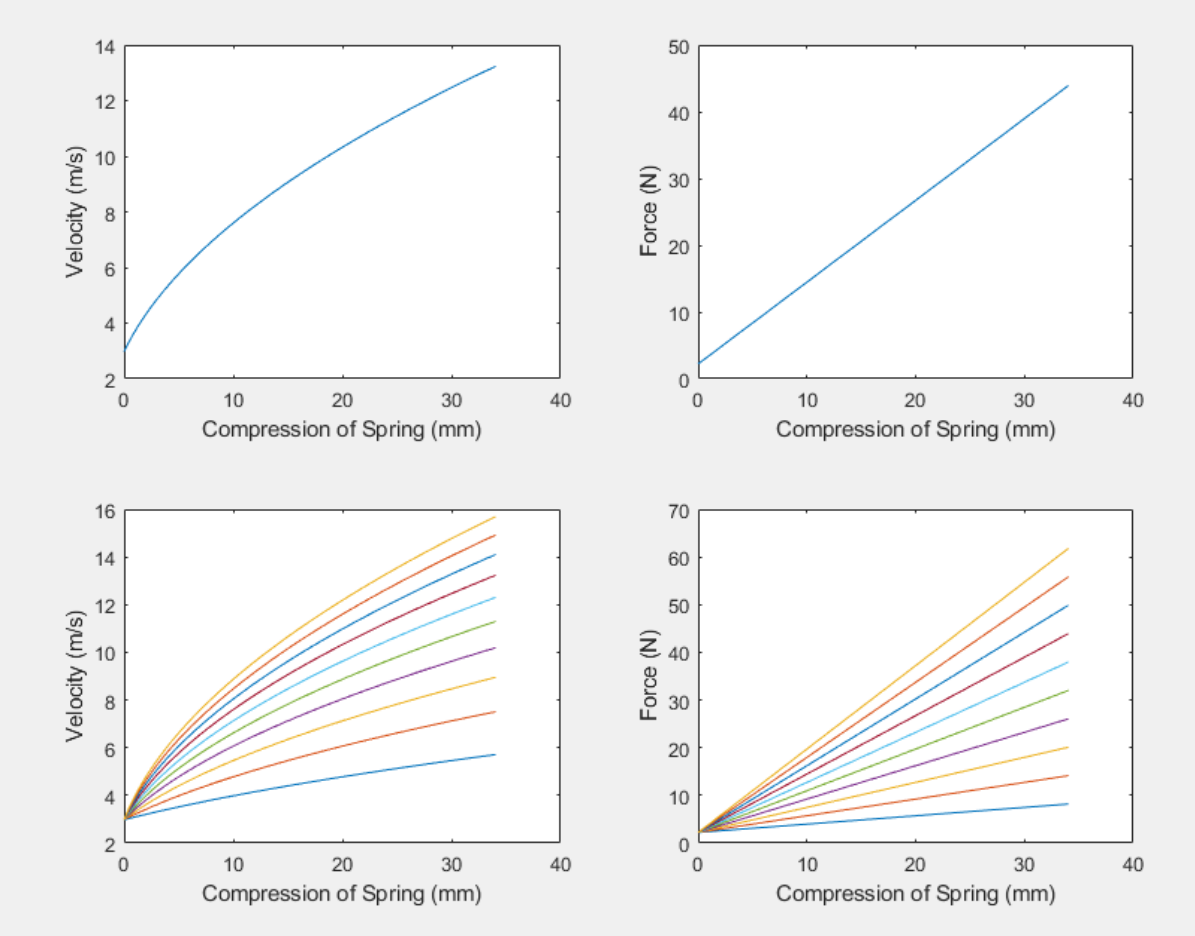


**Figure 2.1:** Force-Velocity Analysis (Top: 7lb-in spring, Bottom: 1 through 10 lb-in springs)

Upon another review, more revisions were to be made. The spring slot on the impactor needed to be aligned with the center of mass of the plate and bracket. The plate and the l-bracket were too heavy, so a combined part that was thinned and cut where material was unnecessary was proposed. There were concerns over guide rail stability, as a larger more stable guide rail and insert could be useful. The top housing was determined to be too large which limited visual and physical access to the organoids at the base. The organoid holder was determined to need a 9 mm spacing between each organoid hole in order to be consistent with the multi-pipette used in the lab which has 9 mm spacing. Additionally, the organoid holder was proposed to have variability in the size of the holes to include a depth of both 0.75 mm and 1 mm, while also including diameters of both 2.4 mm (an additional 20% in size of a 2 mm organoid) and 3

mm (an additional 50% in size of a 2mm organoid). The holder was also to now include channels so that spilled organoid media can flow within the channels and not flow down the square hole of the holder down to the electronics within the base. Lastly, to ensure stability of the holder, a mechanism to pin the holder down must be determined. In the following sections, the final assembly designed via the just mentioned iteration history will be described and illustrated.

*Final Iteration*

Using SOLIDWORKS, the design for this device was modeled. The design can be categorized between a bottom assembly, top assembly, and control system (Figure 2.2). The bottom assembly includes a bottom base, top base, organoid holder, linear stage, linear stage wall, linear actuator, base actuator wall, and eight pins. The top assembly includes a post, impactor tube, guide rail, guide rail insert, impact dropper, l-bracket, magnetic switch, threaded rod, thread knob, spring, and a spring cap. The control system consists of an Arduino, time of flight sensor, and a linear actuator. An exploded view consisting of each part in the overall assembly can be seen in Figure 2.3. Additionally, Table 2.2 provides details about each part, along with their location, material, manufacturer, and purpose within the assembly.

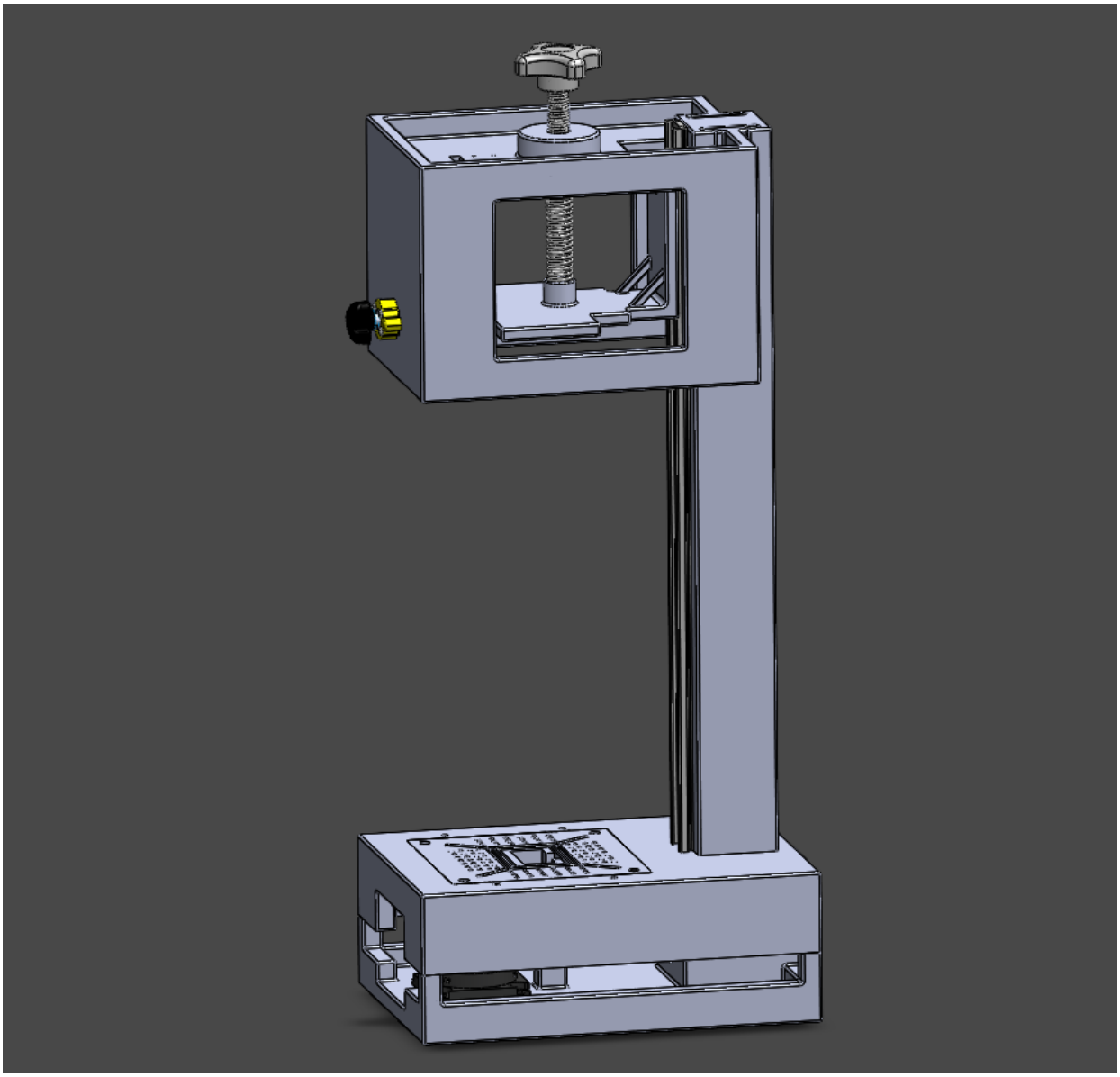

**Figure 2.2:** Overall assembly of organoid impacting device.

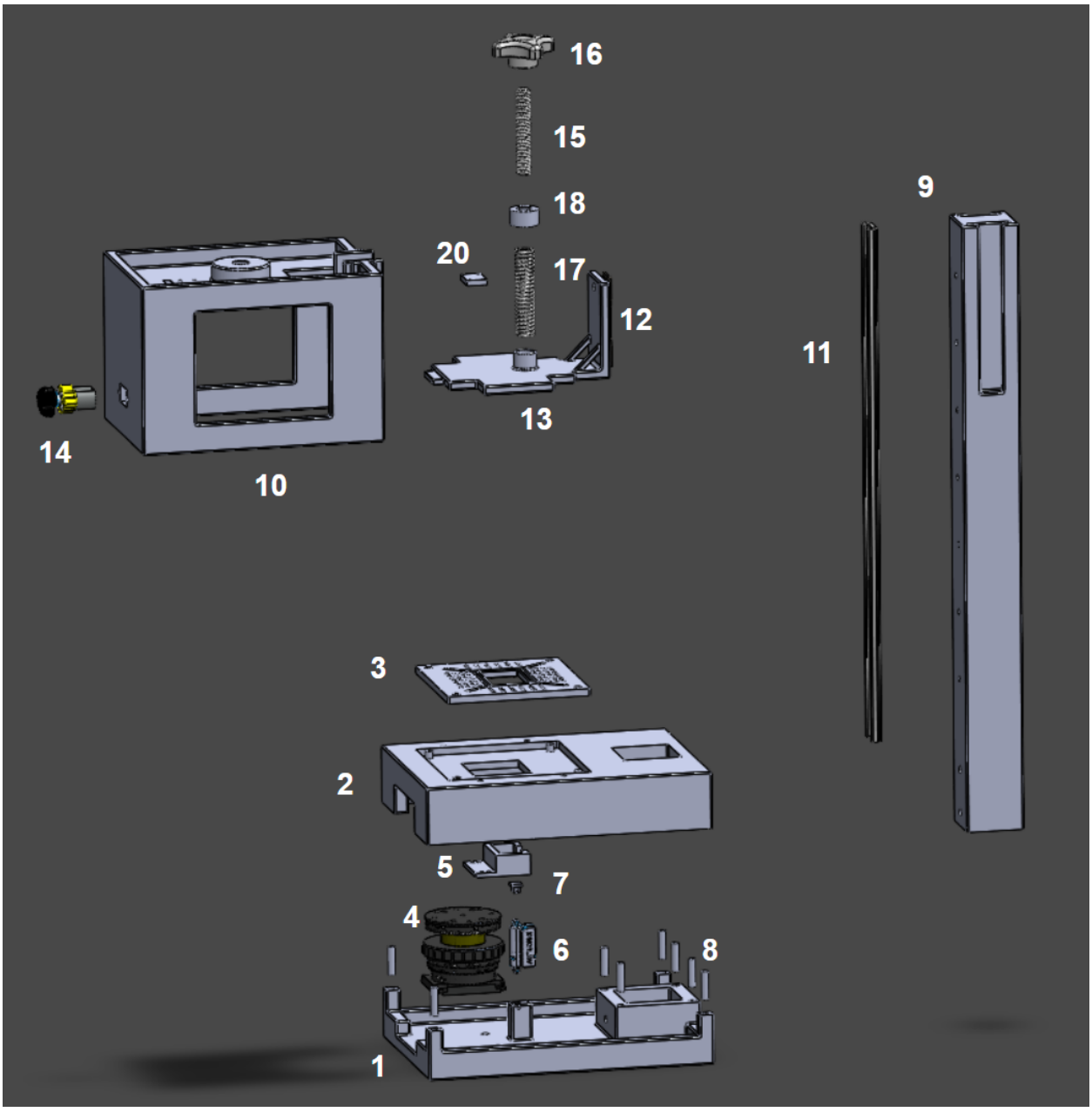


**Figure 2.3:** Exploded view of organoid impacting device.

**Table 2.2:** Subassembly list and details of organoid impacting device parts.

| Part | # | Location | Material/Manufacturer | Purpose | Details |
|---|---|---|---|---|---|
| Bottom Base | 1 | Bottom Assembly | Delrin Plastic (UCSD Machine Shop) | Act as part of the base for the entire assembly, and the base for the linear stage, linear actuator, and the rest of the control system | Dimensions: 254 mm x 177.8 mm x 25.4mm (included with top base) |
| Top Base | 2 | Bottom Assembly | Delrin Plastic (UCSD Machine Shop) | Act as part of the base for the entire assembly, base for the organoid holder, and platform for the impact dropper to impact | Dimensions: 254 mm x 177.8 mm x 25.4mm (included with bottom base) |
| Organoid Holder | 3 | Bottom Assembly | Delrin Plastic (UCSD Machine Shop) | Fit organoids within the holes of the holder for impact | - Includes a center hole for the linear stage attachement and linear actuator<br>- Channels next to the center hole to prevent media spillage into the base<br>- Total holes = 104<br>- Row A: depth = 0.75 mm, diameter = 2.4 mm<br>- Row B: depth = 1.00 mm, diameter = 2.4 mm<br>- Row C: depth = 0.75 mm, diameter = 3.0 mm<br>- Row D: depth = 1.00 mm, diameter = 3.0 mm<br>- 26 holes per type amonst 4 sections<br><br>**Updated organoid holder includes:**<br>- Row A: depth = 0.25 mm, diameter = 1.6 mm<br>- Row B: depth = 0.50 mm, diameter = 2.0 mm<br>- Row C: depth = 0.75 mm, diameter = 2.4 mm<br>- Row D: depth = 1.00 mm, diameter = 3.0 mm |
| Linear Stage | 4 | Bottom Assembly | Thor Labs Compact Lab Jack LJ750 | Influence the fine movement of the linear stage attachment in the z-direction | - High stability lab jack capable of 200lbs of static and active load capacity.<br>- 2" tall when fully collapsed and 3" tall when fully extended<br>- Graduated in 10 um incremements |
| Linear Stage Attachment | 5 | Bottom Assembly | Delrin Plastic (UCSD Machine Shop) | Prevents vibration from impact through its rubber pads at the top surface, and stops the impact dropper at a specific position defined by the linear stage to control the deformation of the organoids | Rubber pads made from O-ring |
| Base Actuator | 6 | Bottom Assembly | Actuonix PQ12-R Micro Linear Servo | Pushes the impact dropperup and away from the organoids directly after impact, so that the organoids do not overdeform | - Works in conjunction with the arduino and TOF sensor<br>- Stroke length of 20 mm<br>- 100:1 gear ratio<br>- Max force lifted = 50 N |
| Base Actuator Attachment | 7 | Bottom Assembly | Delrin Plastic (UCSD Machine Shop) | Acts as a surface of contact between the base actuator and the impact dropper | |
| Pins | 8 | Bottom Assembly | Stainless Steel (UCSD Machine Shop) | Holds the bottom and top base together to prevent shifting, and holds the post and the base together to provide stability | - 8 pins are inserted between the bottom and top base<br>- 2 pins are inserted between the bottom assembly and the post |
| Post | 9 | Top Assembly | Delrin Plastic (UCSD Machine Shop) | Holds the impactor housing up, which consists of the entire spring mechanical assembly, and acts as a surface for the guide rail to attach to | |
| Impactor Housing | 10 | Top Assembly | Delrin Plastic (UCSD Machine Shop) | Provides structural platforms for the spring assembly and magswitch to be attached and loaded | |
| Guide Rail | 11 | Top Assembly | Igus Drylin NK-01-27 Low Profile Linear Slide | Provides vertical guidance for the impact dropper to drop from the impactor housing to the organoid holder | - Length of rail = 458 mm |
| Guide Rail Insert | 12 | Top Assembly | Igus Drylin N - Low Profile Linear Guide System NK-12-27-80 | Attaches the impact dropper to the guide rail for a seamless drop | |
| Impact Dropper | 13 | Top Assembly | Delrin Plastic + Stainless Steel (UCSD Machine Shop | Impacts the organoids at the base to induce injury | - Includes a minimalistic l-bracket to attach to the guide rail insert<br>- Includes a spring slot for the spring to insert<br>- Cuts made where there were no impact on organoids to reduce weight<br>- Delrin plastic is the majority of the body, but at the edge there is a stainless steel attachment that allows for magnetic connection to the magswitch<br>- Weight: 273 g |
| MagSwitch | 14 | Top Assembly | MAGSWITCH MAGJIG 60 – 8100818 | Locks and releases the impact dropper from vertical movement under spring compression | - 2:1 shear working load: 6lbs (2.7 kg) |
| Spring Threaded Rod | 15 | Top Assembly | McMaster-Carr 18-8 Stainless Steel Threaded Rod | Allows for the control of spring compression by rotating the rod down into the spring | - 1/2"-13 |
| Spring Knob | 16 | Top Assembly | McMaster-Carr Four Arm Grip Threaded Hole Knob | Controls the rotation of the spring threaded rod | - 1/2"-13 |
| Spring | 17 | Top Assembly | McMaster-Carr 7 lb-in Compression Spring | Provides additional force for the impact dropper onto the organoids | - 7 lb-in<br>- 3" length |
| Spring Connector | 18 | Top Assembly | Delrin Plastic (UCSD Machine Shop) | Provides connection between the threaded rod and the spring | - One end has a threaded hole for the threaded rod to insert into<br>- Other end has a space to insert the spring and a small pin lock the spring so that it does not fall down |
| Arduino | 19 | Bottom Assembly | Adafruit METRO 328 | Provides an electronic platform to control the base actuator via the TOF sensor | |
| TOF Sensor | 20 | Top Assembly | Adafruit VL53L0X Time of Flight Distance Sensor | Measures the distance between the sensor and the impact dropper and relays it to the arduino to extend the base actuator | - Measures 30 to 1000 mm |

*Fabricated Assembly*

Through the help of the UCSD Machine Shop, the general body of the designed model was fabricated using delrin plastic. Additional parts that were necessary for the assembly were purchased separately, see Table 2.2. Assembling together the body and the purchased parts, a final fabricated prototype of a spring loaded, weight drop, brain organoid impactor device was created, seen in Figure 2.3.

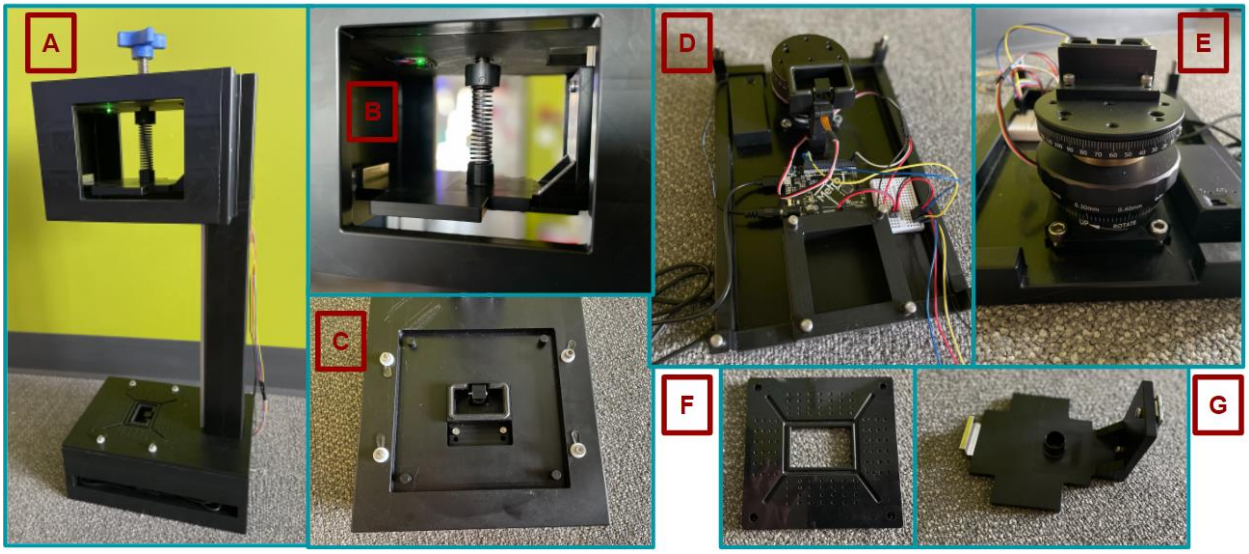


**Figure 2.3:** Final fabricated prototype of brain organoid impactor. (A) Overall assembly. (B) Mechanical assembly (including the impactor dropper, the spring, the stainless-steel attachment, and the TOF sensor) located in the impactor housing. (C) Top base without the organoid holder, showing the base actuator top and the linear actuator attachment. (D) Control system (including the actuator, Arduino, breadboard, wires, and a 9V battery). (E) Linear stage and linear stage attachment. (F) Organoid holder. (G) Impact dropper.

Although the general design was great, during the fabrication of the prototype, slight alterations were made. First of all, in order to manufacture complex parts such as the impactor housing and the impact dropper with ease, the design of these parts was deconstructed and manufactured into separate pieces. These pieces were then reconstructed to form the exact design given. Additionally, on the edge of the impact dropper, a stainless-steel attachment was added to cover the entire surface area of the MagSwitch magnet, in order to combat the shear force generated from the spring and gravity against the MagSwitch. In each of the threaded holes, including the threaded rod hole in the impactor housing and the

holes by the organoid holder, heli-coil attachments were inserted so that the threaded plastic does not wear down with use. To ensure that the spring does not fall after each use, there is a pin inserted into the spring cap and the spring itself. The pins between the top base and the bottom base are also glued to the bottom base, to ensure that each time the base parts are removed from each other, the pins do not fall and get lost. Lastly, a rubber pad, Buna O-Ring, was added to the top surface of the linear stage attachment in order to mitigate vibration from impact to the assembly and organoids.

In addition to these alterations, there were a few challenges in the fabrication and assembly of the prototype. Due to the global pandemic, COVID-19, supply chain disruption delayed the final assembly and testing of the device. The linear stage ordered from Thor Labs arrived a couple of months later than expected, after extensive talks with customer service and technical support. In terms of fabrication, the post and the base parts were manufactured as a very tight fit which requires delicate force in order to take apart. Lastly, the impact dropper had some surface roughness after initial fabrication and required further inspection and alteration to ensure surface flatness at the bottom surface of the dropper.

*Control System*

The control system for this device includes an adafruit arduino, an adafruit TOF sensor, and an actuonix actuator. The TOF sensor measures the distance of the impact dropper from the top of the impactor housing, and once the dropper reaches a specific distance, the arduino activates the actuator to extend right after the dropper makes impact. The actuator extending pushes the impact dropper to just above the organoids so that it does not induce constant deformation. In Figure 2.4, a diagram of the control system logic is illustrated and explained.

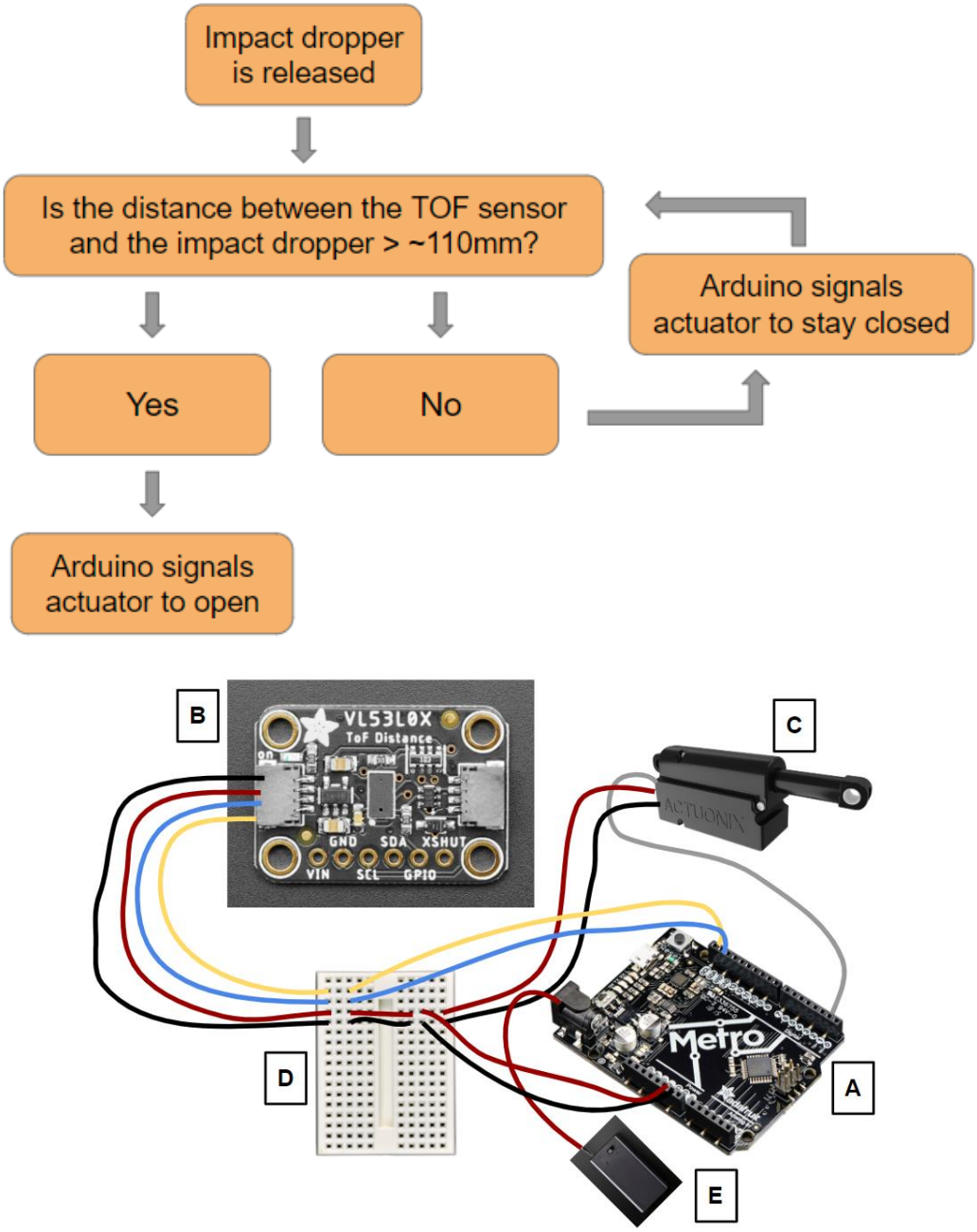


**Figure 2.4:** Control system logic (top) and diagram (bottom): (A) Arduino, (B) TOF Sensor, (C) Linear Actuator, (D) Breadboard, (E) 9V battery. The TOF sensor provides distance metrics to the Arduino which activates the linear actuator.

Although the control system is quite simple, there were some challenges and iterations. The first iteration required a soldered contact between the sensor and the Arduino, but after over-soldering the first TOF sensor was fried. The second TOF sensor was soldered and worked perfectly fine, but it was found

that the sensor could only detect up to 100 mm, when over 300 mm was needed. A similar TOF sensor, but with a sensor distance of up to 1000 mm and a non-soldering wire attachment, was purchased and connected to the Arduino. The challenge here was that multiple purchases were made for the numerous TOF sensors and wires that were able to reach the top of the assembly, which further delayed testing and production. In addition, there were many iterations in developing the code to logically connect the sensor and the actuator and to calibrate the timing so that the actuator extends right after the dropper impacts.

With respect to the code, the main features include setting up the TOF sensor and the actuator to be connected, setting the distance from the sensor for when the actuator must open, and setting up the range for the actuator to open and close. The actuator has two functions: open and close. The values that correspond to these functions are 1000 to 2000, respectively. These values are a range that the actuator can open to. For example, if the value is 15000, the actuator is halfway open. For this project the open value is set to 1000, but the close value is set to a varying value that is determined by the calibration of the drop, making the actuator closer to the impact surface (since it comes from below). In addition, the TOF sensor has a sensing range of 0 to 1000 mm. By altering the value of which the TOF sensor signals the actuator to open, the impact drop can also be calibrated. Lastly, a delay is necessary to ensure the actuator completes its action before the next signal. The code for this system can be found in Appendix 3.

# METHODS

## Phantom Organoid Testing Methods

Specific tests were run using phantom organoids in order to validate the accuracy and efficacy of the device model. The main goal in these tests is to determine whether or not the device establishes deformation control of the brain organoids. Phantom organoids made out of play-doh formed approximately 2 mm sized balls to mimic the size of brain organoids, acting as a substitute. In the following section, methods of testing and analysis are discussed.

### *General Testing Protocol & Rationale*

As introduced before, in Table 2.2 and Figure 2.3, the organoid holder has numerous wells that differ in location, depth, and diameter. In the following tests, approximately 2 mm phantom organoids were formed out of play-doh, measured in diameter using calipers, and inserted into the wells of the organoid holder. A small water-based ink drop was placed on top of the phantom organoids, and a piece of paper was taped to the bottom surface of the impact dropper. The rationale of the ink and paper is that when the impact dropper hits the phantom organoids, the ink will leave an imprint on the paper taped to the bottom surface of the dropper. When the ink drop on the phantom organoid hits the dropper the phantom organoid deforms and expands, therefore expanding the imprint left on the paper. Following the impact, the diameter of the imprint is measured, which will be compared to the initial diameter of the phantom organoid in order to calculate percent deformation of the phantom organoid post-impact.

### *Deformation Analysis*

Once the two diameter measurements have been recorded, the calculation of the percent deformation post-impact is determined through an equation utilizing the area of a circle and the spherical cap theory. The assumptions that were made in order to use this calculation is that the ink droplet covers the entire range of deformation on the imprint, that the phantom organoids are close to perfectly spherical, and that the phantom organoids are unconfined laterally. With this in mind, the spherical cap theory states

that the surface area of the spherical cap is equal to 2*R*h, which is illustrated in Figure 3.1. This formula represents the initial state of the phantom organoid, pre-impact, whereas the formula of the area of a circle represents the projection of the final state of the phantom organoid, post-impact. Setting these two equations equal to each other, it is possible to solve for the height of the spherical cap and compare it to the original diameter of the phantom organoid to calculate percent deformation.

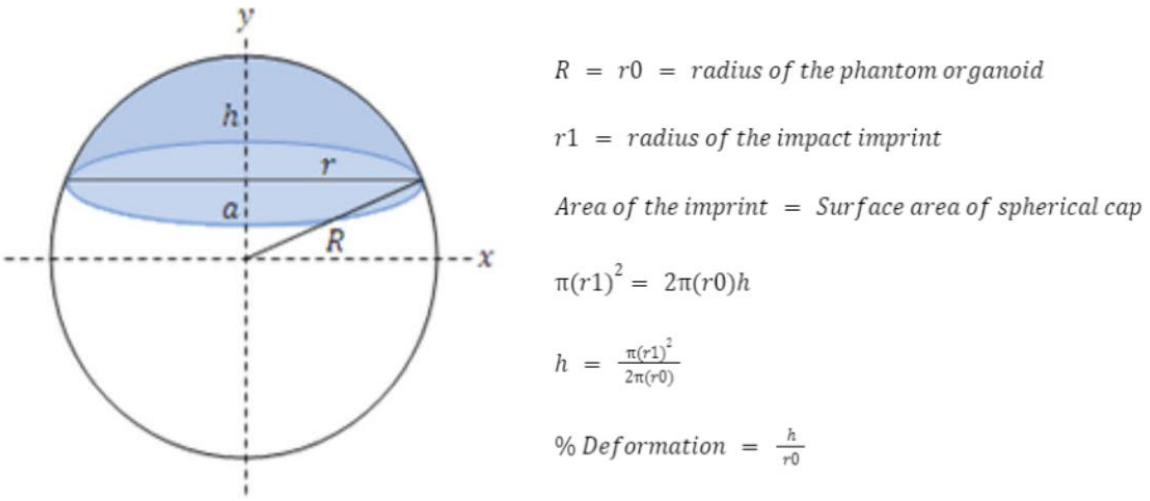


**Figure 3.1:** Spherical cap theory illustration and equations. R represents the radius of the entire sphere, r represents the radius of the spherical cap, and h represents the height of the spherical cap.

In addition to the actual deformation analysis, theoretical deformation analysis can be done. In Figure 3.2, a theoretical schematic illustrates how much deformation can be expected in these tests. When calculating theoretical percent deformation, the organoid diameter, the stopper height (the linear stage attachment), and the well depth is taken into account. Subtracting the stopper height and well depth from the organoid diameter should represent the remaining material that the organoid can be deformed. By dividing that remaining amount by the total organoid diameter, the theoretical % deformation can be calculated. The values considered for the stopper height are 0 mm, 0.5 mm, 1.0mm, and 1.5mm. The values considered for well size included 0.75 mm and 1.0 mm. The values considered for organoid diameter are 1.75 mm and 2.25 mm.

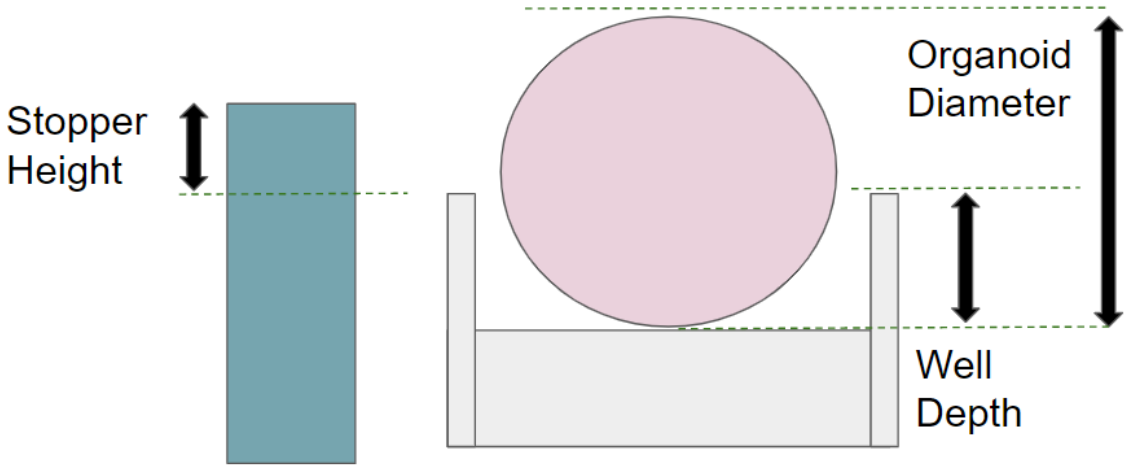


$$Theoretical\ \%\ Deformation\ =\ \frac{Organoid\ Diameter - Stopper\ Height - Well\ Depth}{Organoid\ Diameter}$$

**Figure 3.2:** Theoretical organoid impact schematic and theoretical % deformation equation.

*Initial Testing*

Prior to the actual testing, initial tests were run in order to provide data allowing us to determine the best method to calculate and analyze percent deformation, as seen above. There were 7 total tests, consisting of 96 phantom organoids total. There was no rationale behind each test, other than trying different locations in the organoid holder, and different sized phantom organoids. Procuring this data allowed the researcher to become comfortable and efficient with the testing procedure, and to provide data to analyze using different methods. Other than the spherical cap theory method listed above, two other methods were considered. The first method was a great tool to approximate percent deformation, but was not specific enough. This method assumes that if the surface area of half of the phantom organoid is 50 percent, then using the imprint area of the impacted phantom organoid, percent deformation can be approximated using proportional analysis. The second method, similar to the current method, utilizes the spherical cap theory in combination with the Pythagorean theorem to calculate the height. The triangle seen in Figure 3.1, illustrates the triangle used in the Pythagorean theorem which develops into a quadratic that can be used to solve for height. This method provided eerily similar results to the current

method, but it exaggerated certain data, which was theoretically not possible. Thanks to the initial testing, the data generated determined these methods as inaccurate in comparison to the current method described above. In the following sections testing was done to answer the following questions to determine the accuracy and efficacy of the impact device: how does the spatial position of organoid placement affect deformation, how does the stopper height affect deformation, and how does the compression of the spring affect deformation.

*Spatial Positioning*

After determining the best method to calculate and analyze percent deformation, a series of tests were run to determine how the spatial position of organoid placement affects deformation. As introduced before, in Table 2.2 and Figure 2.3, the organoid holder has numerous wells that differ in location, depth, and diameter. There are a total of 104 holes separated by 4 regions (front, left, back, right). Each region has 4 rows that will be labeled as Row A through D from the inner row to the outer row, respectively, illustrated in Figure 3.3. Each hole in the specific row is numbered from 1 through 6 or 7 depending on the region. Rows A and B have diameters of 2.4 mm, but have depths of 0.75 mm and 1 mm, respectively. Rows C and D have diameters of 3 mm, but have depths of 0.75 mm and 1 mm, respectively. The variety of size in holes allows the researcher to use any organoid, regardless of the variable sizes per batch.

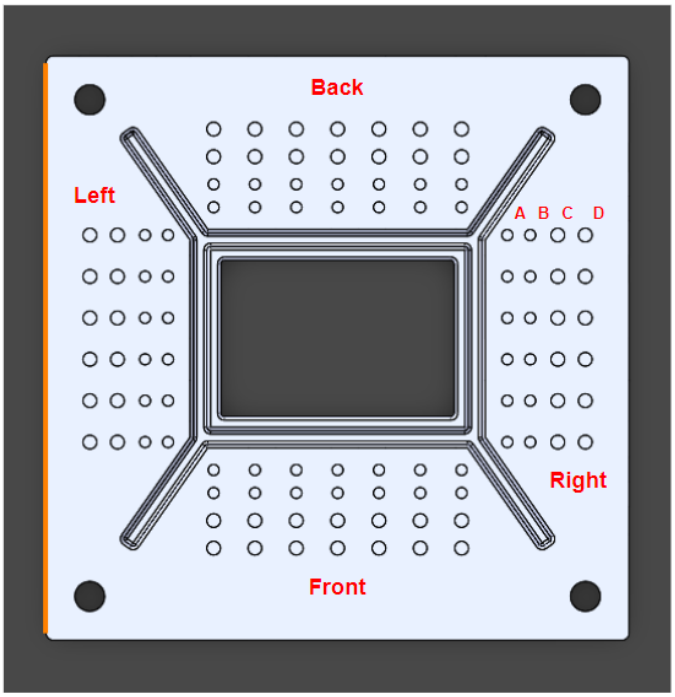


**Figure 3.3:** Organoid holder positional labeling.

With this in mind, the tests on spatial positioning consisted of 8 drops. Every 2 drops tested a specific row in all sections, with 5 phantom organoids per row, adding up to 20 phantom organoids per test. Drops 1 and 2 tested row A, drops 3 and 4 tested row B, drops 5 and 6 tested row C, and drops 7 and 8 tested row D. The total sample size of these series of tests was 160 phantom organoids. The stopper height was positioned at 1mm above the surface of the organoid holder, and there was no spring compression. The phantom organoids in rows A and B were sized between 1.5 and 2 mm in diameter, and in rows C and D they were sized between 2 and 2.5 mm. After testing was done, consisting of diameter measurements of the pre-impact organoid and the imprint area, data was compiled to illustrate differences in deformation by row and region. Sample test positioning and imprint imaging is seen in Figure 3.4.

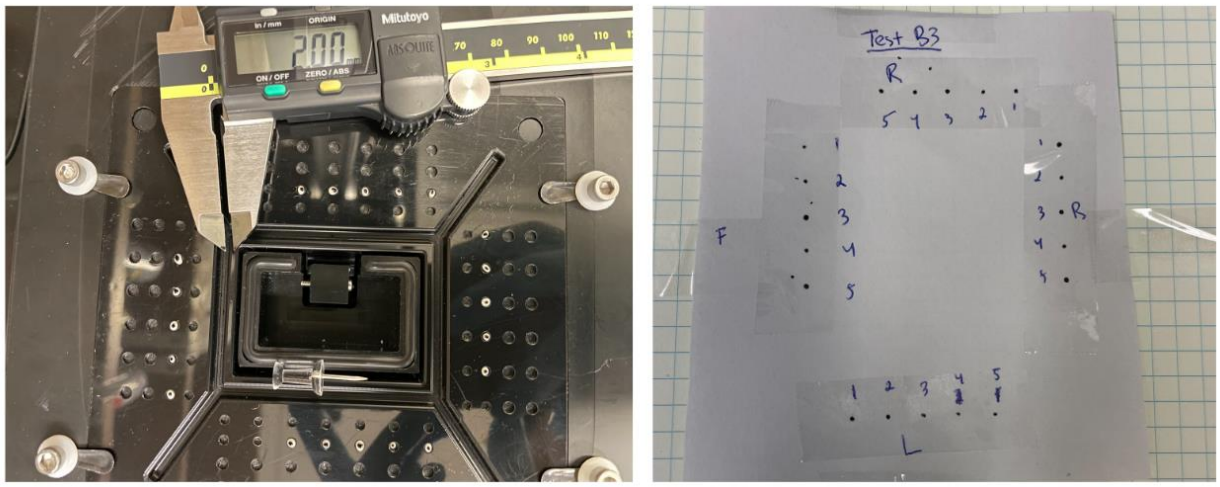


**Figure 3.4:** Sample spatial test positioning and imprint imaging. (Left) Positioning of phantom organoids for a sample spatial positioning test, including the ink droplets and scaling. (Right) Impacted imprints labeled by position.

*Stopper Height*

Next, a series of tests were run to determine the effect of stopper height on deformation. Represented by the linear stage attachment, the stopper is controlled by the linear stage in very fine height measurements to the micrometer. The stopper height, as illustrated by Figure 3.2, is the height of the linear stage attachment above the organoid holder surface. Similar to the spatial positioning tests, 8 total drops were run, consisting of 160 total phantom organoids. Each drop consisted of 20 phantom organoids positioned in the right region. The drops differed in stopper height as drops 1 and 2 were at 0 mm, drops 3 and 4 were at 0.5 mm, drops 5 and 6 were at 1 mm, and drops 7 and 8 were at 1.5 mm. The organoid sizes followed the same trend as the spatial positioning tests. Sample test positioning and imprint imaging is seen in Figure 3.5. The data compiled from these tests then illustrated differences in deformation by overall stopper height and by stopper height differences per row. The results of this data exposed differences between the experimental data and the theoretical data. More specifically, the % deformation from the 0 mm experimental data was noticeably less than the 0 mm theoretical data. The hypothesis as to why this occurred was that the ink droplet placed on the phantom organoid did not measure the accurate deformation, as the deformation was greater than the amount of ink placed. With this in mind, the 0 mm tests were rerun covering the phantom organoids with better ink coverage.

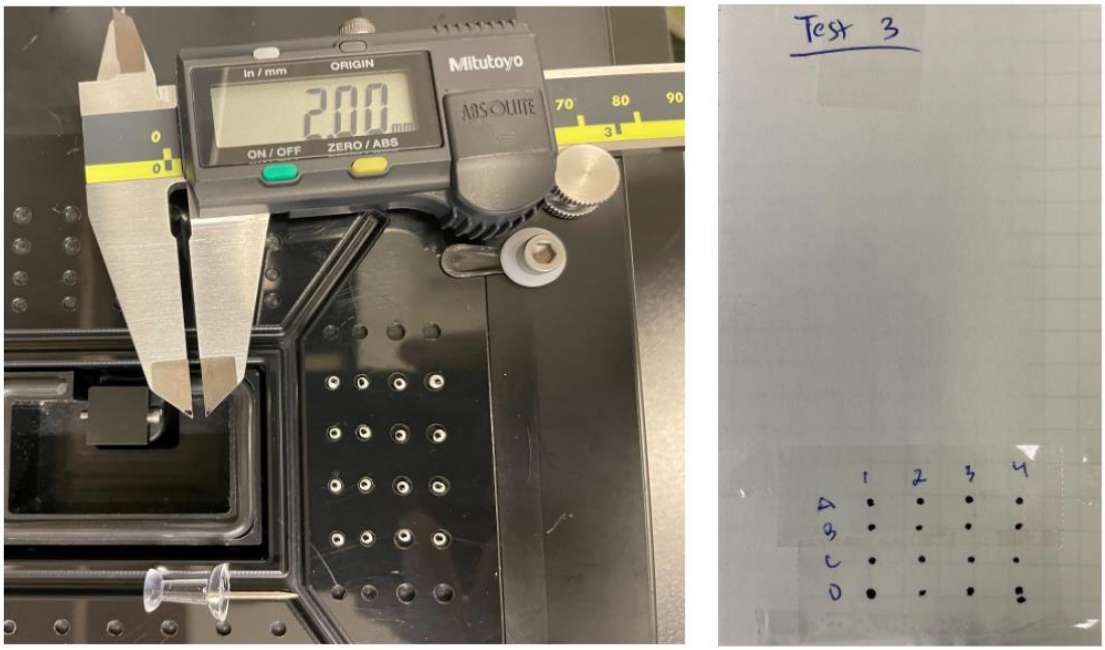


**Figure 3.5:** Sample stopper height test positioning and imprint imaging. (Left) Positioning of phantom organoids for a sample stopper height test, including the ink droplets and scaling. (Right) Impacted imprints labeled by position.

*Spring Compression*

In the final series of tests, the effect of spring compression on percent deformation was determined. As the main control over velocity and force in impacting brain organoids to induce TBI, spring compression is hypothesized to have no effect on deformation percentages, rather just induce greater damage to the brain organoids. To confirm this, a single test was run to determine whether or not this hypothesis was valid. This test consisted of 20 total phantom organoids, 5 in one row for each region. The stopper height was set to 1 mm, to allow for comparison to the spatial positioning tests. In previous experiments, there has been no spring compression generating a calculated velocity and force of 2.97 m/s and 2.68 N, respectively. Here, the spring was compressed 15.47 mm, which is the approximate maximum compression that the magnetic lock can withstand, generating a calculated velocity and force of 8.45 m/s and 21.63 N, respectively. The data compiled from this test was then compared to the data generated from the spatial positioning tests, looking for any significant difference in deformation percentage. Differences in spring compression can be seen in Figure 3.6.

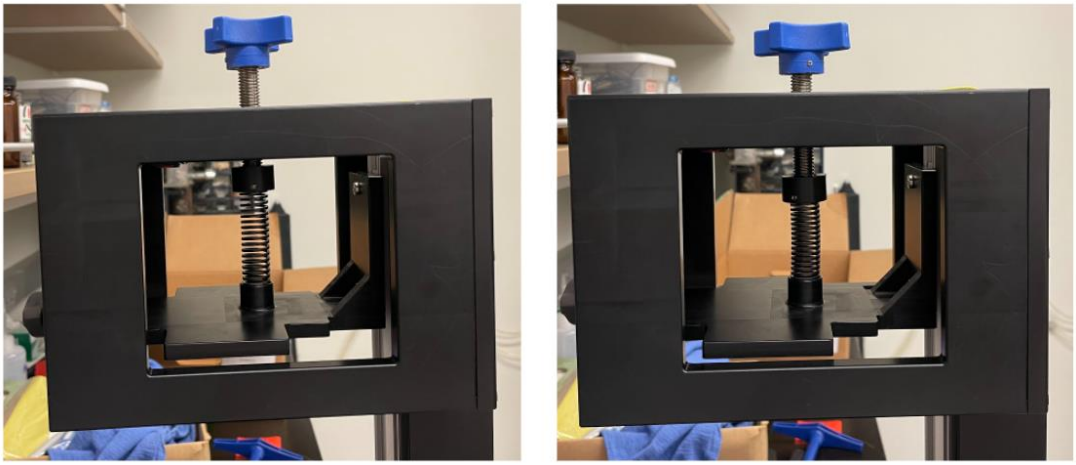

**Figure 3.6:** Sample spring compression images. (Left) Spring uncompressed. (Right) Spring compressed.

## Brain Organoid Testing Methods

### *Preliminary Trials*

After testing with the phantom organoids, real brain organoids were next. The device was first sterilized and decontaminated using 70% EthOH. In addition, the parts that were to contact the organoids (i.e., the impact dropper and the organoid holder) were treated with UV exposure for about 10-15 minutes. Once decontamination was complete, the device was re-assembled and placed in the hood, shown in Figure 3.7.

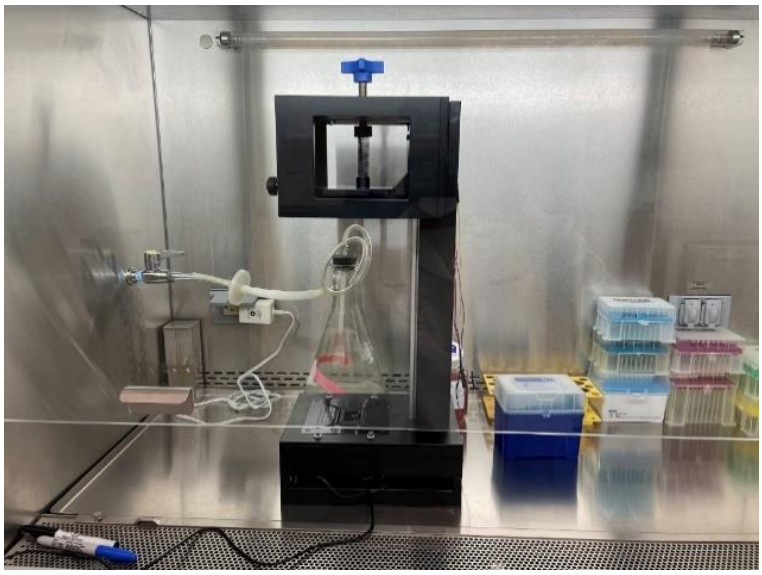

**Figure 3.7:** Assembled organoid impacting device placed within a hood.

The purpose of these preliminary trials was to calibrate the device for the nature of the organoids, in contrast to the phantom play-doh organoids used prior. A total of 8 tests were run initially, with 1 organoid used per test. It was observed that the organoids were smaller than expected and measured between 1 mm to 1.5 mm (versus the expected ~2 mm sized organoids). Between each test the stopper height differed to monitor the true effects of the impactor against the organoid, and provided valuable information on what stopper height was necessary to generate the results expected for future experiments. These initial experiments posed concerns of the device including: the wells in the organoid holder are too deep for the organoids, at a stopper height below 0.2 mm the organoids get crushed beyond use, and the organoids like to stick to the impact plate after the impact. Each of these concerns posed sources of variability in our experiments and needed to be resolved before further testing ensued.

In addition to the previous sized wells, an improved organoid holder, seen in Figure 3.8, was designed to include wells with the sizes of 1.6 mm and 2.0 mm in diameter and 0.25 mm and 0.5 mm in depth, respectively. A bio-safe Teflon spray was also introduced to ensure the organoids don't stick to the impact dropper. To estimate how much deformation the organoids were being placed under, another theoretical calculation was made. Similar to the previous theoretical calculations (figure XX), the new organoid height, stopper height, and new well depth was utilized to solve for percent deformation. It can be established that based on the results from the phantom organoid testing, theoretical analysis estimates similar deformation percentages.

Using the improved organoid holder, a total of 15 tests were run, with 1 organoid per test. The row that had 0.5 mm in depth was used for each of the tests. The stopper height was varied to test the injury limits of the organoid, and to reveal the best candidate for a positive control, where the damage on the organoids is clearly seen but it does not stick to the impact dropper. In addition, spring force was added to check the range of damage it could further induce, and check its viability to be added to the positive control candidate. The calculated velocity and force of no spring compression is 2.97 m/s and 2.68 N, respectively. The spring was compressed 14.04 mm, generating a calculated velocity and force of

8.08 m/s and 19.78 N, respectively. A couple challenges that arose during these tests included that the organoids were even more difficult to remove using a pipette since the organoid wells became smaller, and that depending on the damage to the organoid, it would sometimes stick to the inside of the pipette needing to be washed down by media to remove. In addition, the Teflon spray did not seem to have any effect as the organoids still stuck to the impact dropper depending on the amount of surface area in contact, which is varied by the stopper height.

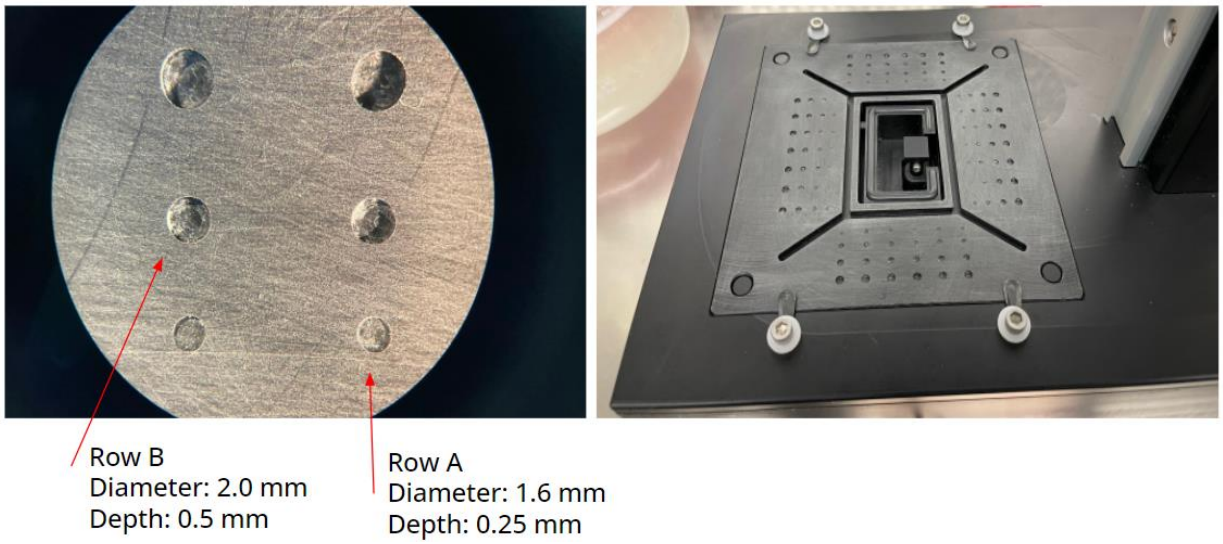


**Figure 3.8:** Improved organoid holder. Row A now has a diameter of 1.6 mm and a depth of 0.25 mm for extremely small organoids. Row B now has a diameter of 2.0 mm and a depth of 0.5 mm for normal sized organoids. Row C has a diameter of 2.4 mm and a depth of 0.75 mm for larger sized organoids. Row D has a diameter of 3.0 mm and a depth of 1.0 mm for potential fused organoids.

*Final Protocol*

The following tests will include a positive control, a negative control, and two test groups. The general protocol for each of these tests will be as followed, using the new organoid holder. Organoids will be removed from their incubator and transferred to a multiple well dish with one organoid per well. These organoids will be photographed using the EVOS imager for pre-impact imaging, and transferred to the hood where the device is set up. As for the device, it is sterilized and decontaminated using 70% EthOH, and the impact dropper and the organoid holder were treated with UV exposure for about 10-15 minutes.

After decontamination the device was re-assembled and placed in the hood. Re-assembly consists of placing the impact dropper within the guide rail, placing the impact housing on top of the post and magnetically locking the impact dropper, fitting the organoid holder on the base and pushing the flaps across to ensure it is level, and turning on the Arduino battery. Next, the stopper height is checked to ensure it is first at 0 mm and then can be increased to whatever stopper height is chosen, and the spring is checked to ensure it is either uncompressed or compressed, depending on the test. In addition, the Arduino code is re-uploaded to the calibrated timing for each stopper height and drop. Once these device checks are complete, the organoids can be placed within the organoid holder wells. For the following tests, 3 organoids are used per test and are placed into the wells. Images are taken from the top and on the side to clearly show the organoids in their respective wells. Next the magnetic lock is released and the impact dropper hits the organoids and is lifted up by the actuator. The organoids are then carefully removed from the well and photographed in the EVOS imager for post-impact imaging. The organoids are then placed back into the incubator for further immunohistochemistry (IHC) staining and imaging.

*IHC Staining*

The following fluorescent stains will be placed upon each of the test groups: DAPI, GFAP, Caspase-3, and Neurofilament-200. DAPI binds to regions in the DNA and will serve as an indicator for nuclei in the neuronal cell. GFAP binds to glial cells and will serve as an indicator of glial cell stress and astrocyte activation. Caspase 3 binds to caspase proteases that initiate and execute apoptosis and will serve as a cell damage and death indicator. Neurofilament binds to the cytoskeleton of the neuron and will serve as a structural marker.

Prior to IHC staining, the brain organoids within each test group were sectioned at 10 microns. These sections were then hydrated in 1X PBS for approximately 2 minutes, and were then blocked for 1 hour in 2% BSA, 5% serum of secondary antibody, and 0.1% TritonX-100. Then each of the antibodies, both 1/500 dilution in block, were added and incubated overnight. The next day, the sections were washed 3 times with 1X PBS, applied with the secondary (1/500 in 1X PBS) for 1 hour at room temperature,

washed an additional 3 times, and was then mounted with Fluoromount-G. The sections were then imaged using a Nikon fluorescent microscope. In addition to the stains described above, additional unstained sections were imaged to check for any background signaling, indicating there was minimal to no background signaling.

## Phantom Organoid Testing

### *Spatial Positioning*

The first series of phantom organoid testing determined to answer whether or not the spatial position of organoid placement on the organoid holder affects deformation. Figure 4.1 - 4.3 demonstrates the differences in deformation by row, region, and a combination of both row and region. It is important to note that the differences in deformation by row are measuring the intentional changes made by the experimenter, as each row is different in deformation. This allows the user to know whether or not intentionally using different rows will affect deformation. On the other hand, differences in deformation by region are measuring design related changes that can only be altered through different design and fabrication. These regions are expected to have no difference as the design is also expected to have no difference by region. This will allow the user to know if there are any limitations in the design.

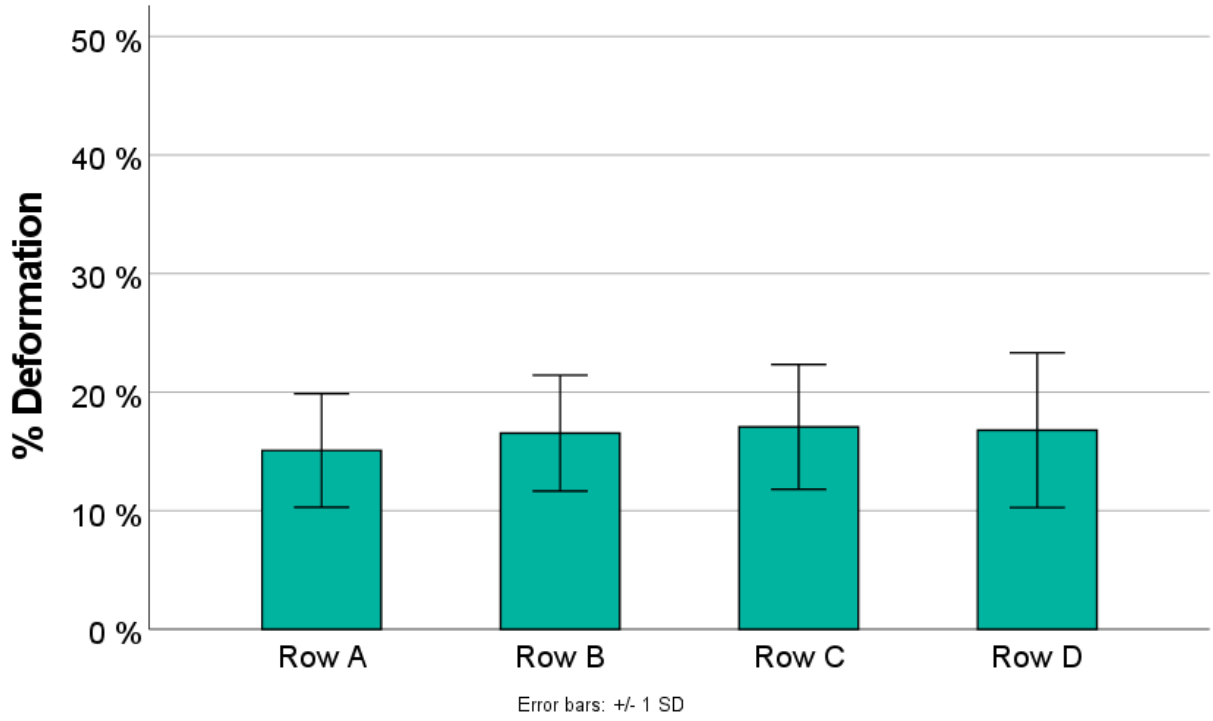


**Figure 4.1:** Row spatial positioning effect over phantom organoid % deformation.

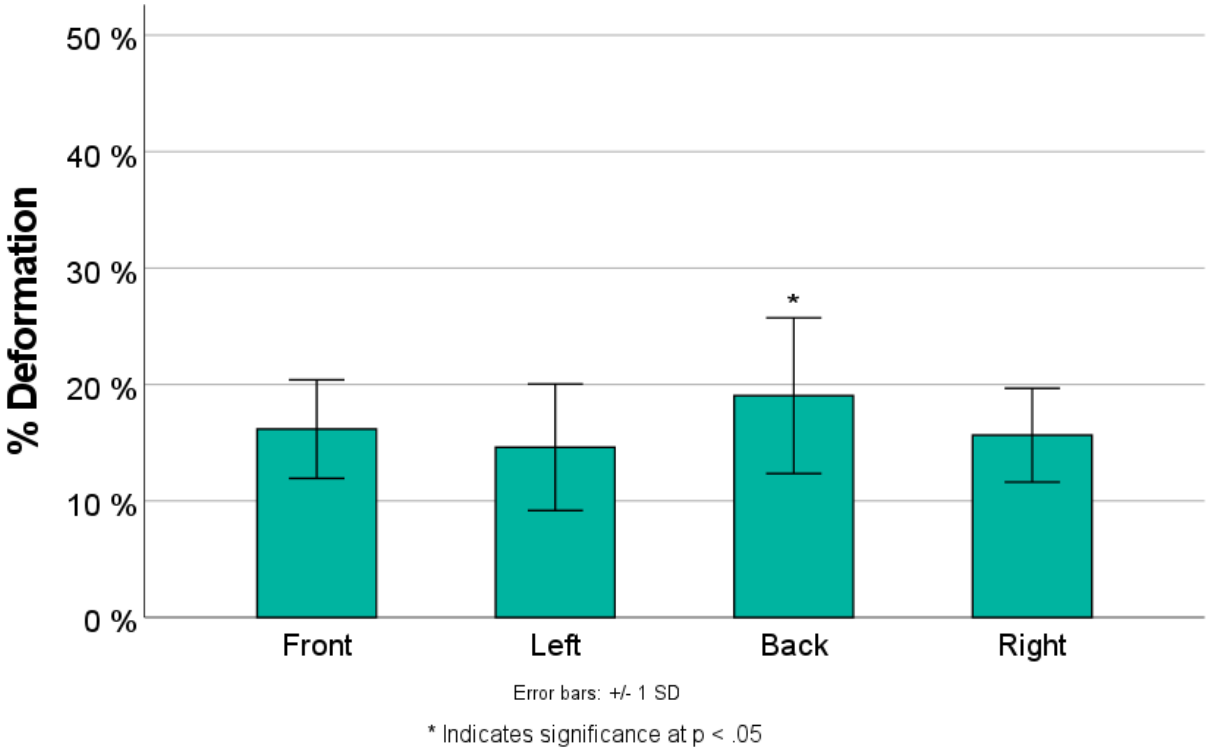


**Figure 4.2:** Regional spatial positioning effect over phantom organoid % deformation.

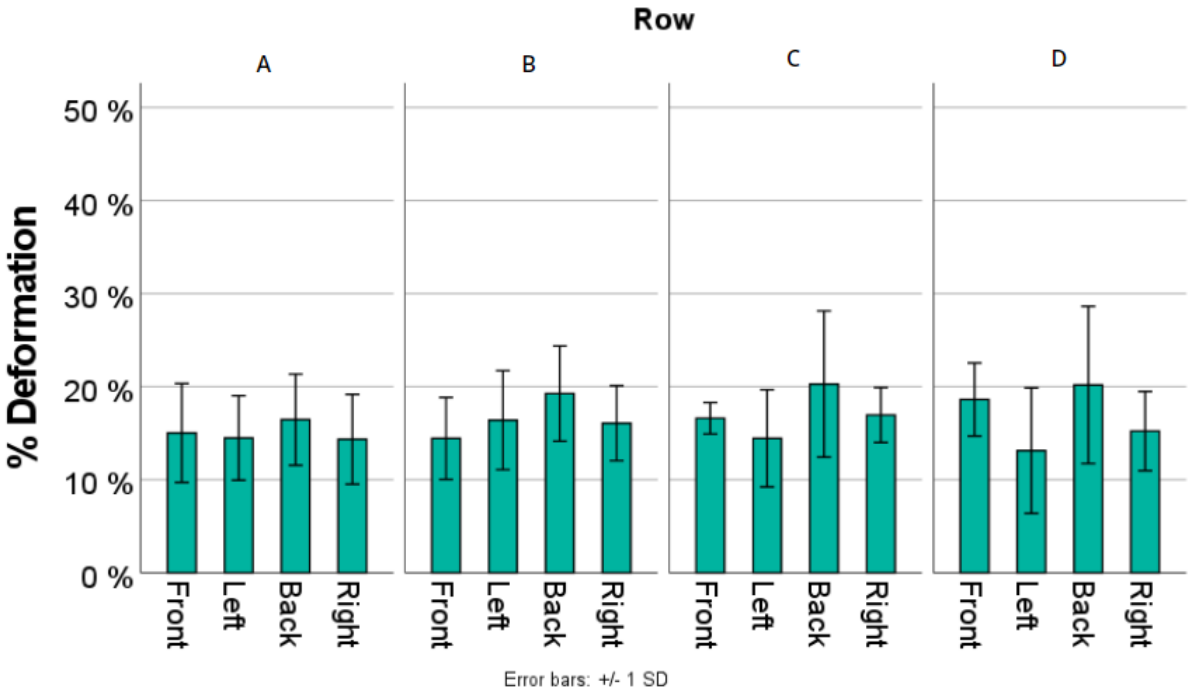


**Figure 4.3:** Spatial positioning effect over phantom organoid % deformation by region per row.

Based on Figure 4.1, there seems to be no significant difference between rows as they all produce similar deformation percentages. This indicates that by intentionally changing the row has no impact on altering deformation percentages, using similarly sized phantom organoids. In addition, based on Figure 4.2, all the regions, except the back region, seem to have no difference in deformation. The significant increase in deformation in the back region ($p < 0.05$) indicates that there is a limitation and flaw in the design that is leading to the back region generating greater deformation. It is hypothesized to be due to the impact dropper hitting the base at a slight slant, impacting the back region first before hitting the others. With this in mind, future experiments will refrain from using the back region until a new design can be generated. Lastly, Figure 4.3 illustrates that spatial positioning by region per row is not significantly different in deformation percentages. This is meaningful because it means that the user could perform their experiments with only one row across each region and not have to worry about major differences. Despite not being significantly different, there is still a marginal difference between the back region and the rest of the regions, further confirming that the region should no longer be used. Overall, the trend illustrated by these results indicates that spatial positioning of the organoids, by row or region, (excluding the back region) does not make any difference. This confirms the ability of the device to produce similar deformation amongst a multitude of organoids in bulk from a single test

*Stopper Height*

The next series of phantom organoid testing determined to answer whether or not the stopper height affects deformation. Figure 4.4 illustrates the theoretical stopper height effect on deformation for varying well depths and organoid sizes. Initially, before the theoretical analysis, tests varying stopper height were performed, and this theoretical analysis allowed for a comparison check to ensure our experimental results matched similarly. This comparison found that our initial tests for the 0 mm stopper height were flawed and needed to be run again using a different method.

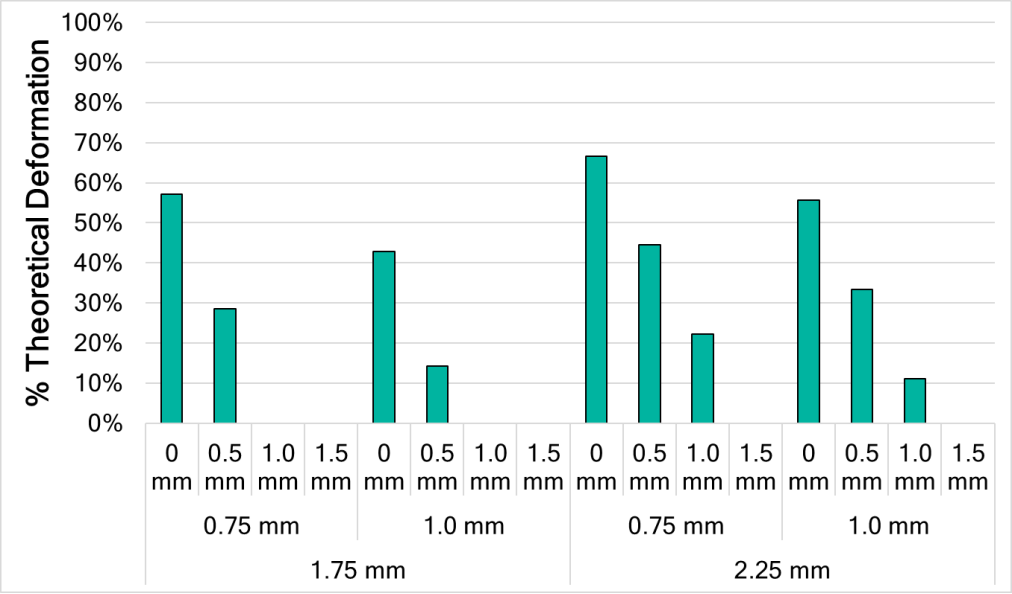


**Figure 4.4:** Theoretical % deformation of phantom organoids by stopper height. Variables differentiated on the x-axis consist of theoretical organoid diameter (bottom x-axis), well depth (middle x-axis), and stopper height (top x-axis), which all are used in calculating the theoretical % deformation.

Inclusive of the new method for the 0 mm stopper height, Figure 4.5 demonstrates that experimental deformation percentages decrease as stopper height increases. The trend in these results correspond well to the expected results seen in the theoretical analysis, and illustrate a significant difference ($p < 0.01$) when using a 0 mm stopper height. As the stopper height increases, the deformation decreases, which is also expected. This confirms that the stopper mechanism in the design works as planned and that through the control of the stopper height, organoid deformation can be easily manipulated. Figure 4.6 illustrates a breakdown by of stopper height deformation differences by row, which further demonstrates that there is no significant difference between rows. With this in mind, we are confident that this device can control deformation from a range of ~60% to less than ~10%, with a variance of 5%. In combination with the organoid holder results, we are also confident that this device can achieve the expected requirements that allows for variable and efficient experimental use.

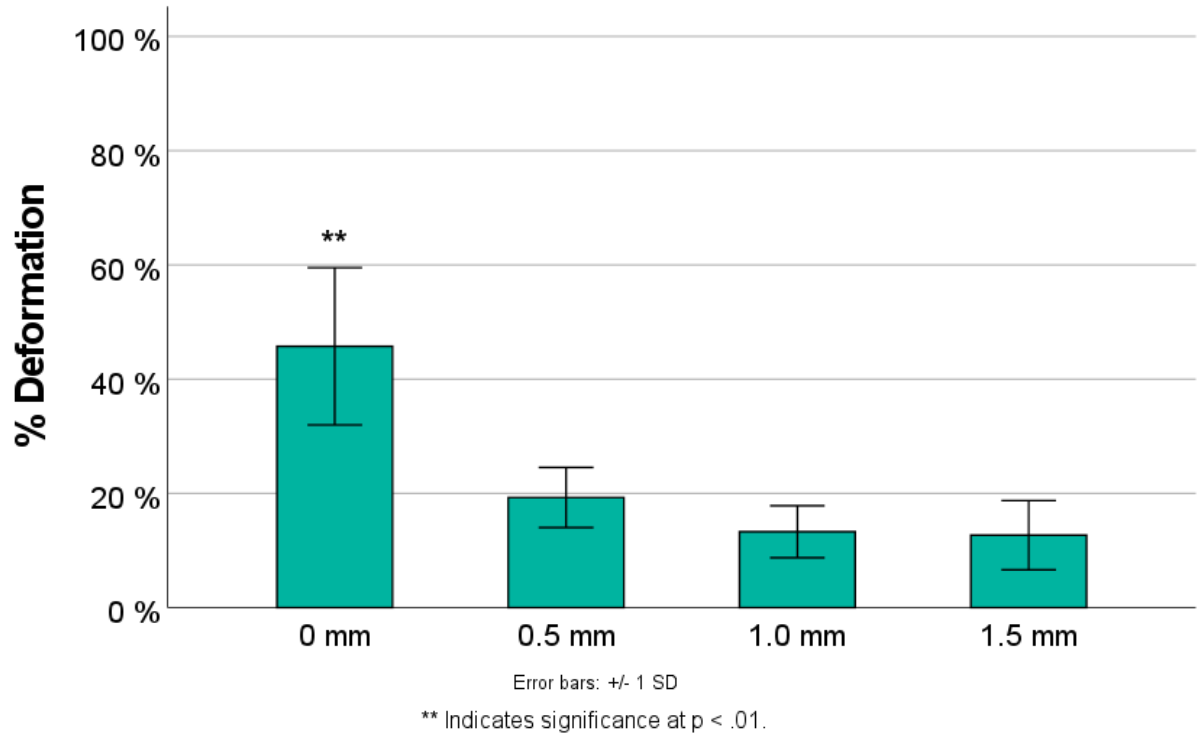


**Figure 4.5:** Stopper height effect over phantom organoid % deformation.

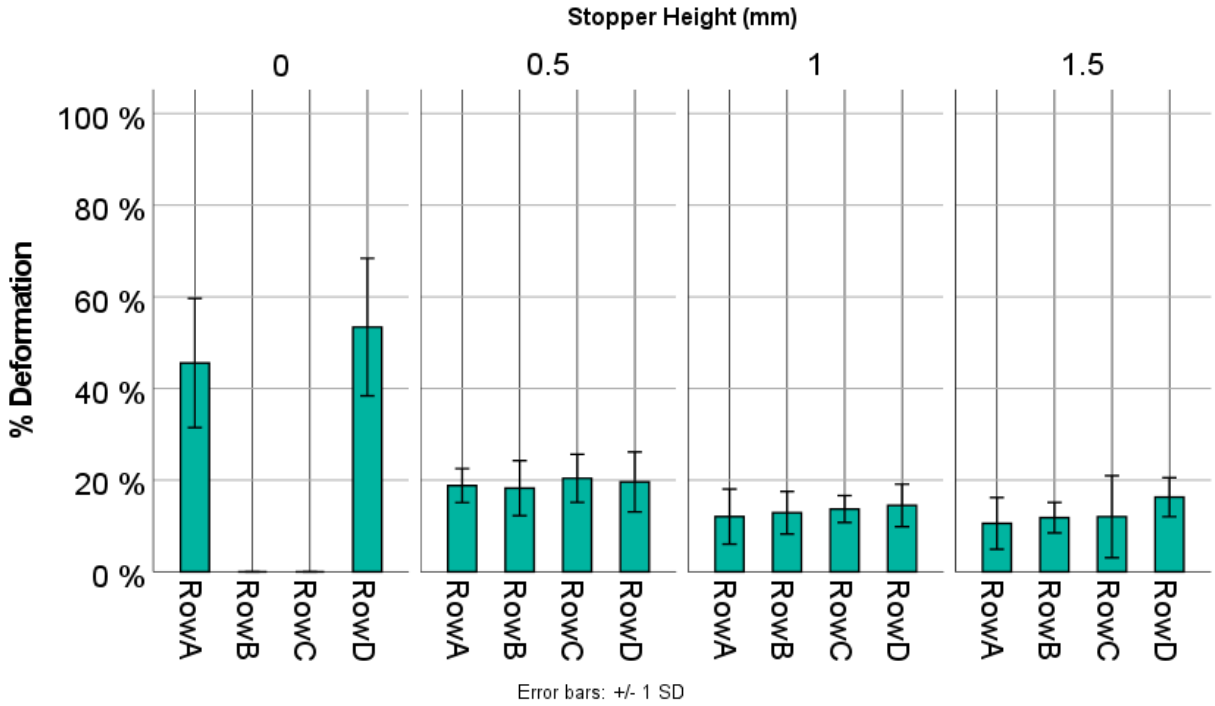


**Figure 4.6:** Stopper height effect by row over phantom organoid % deformation.

*Spring Compression*

The final series of phantom organoid testing determined to answer whether or not the compression of the spring, therefore inducing greater force, affects deformation. Figure 4.7 illustrates that there is no difference in deformation percentages when compressing the spring. This confirms the expected results as only the stopper height is meant to have control over the organoid deformation, while the compression of the spring is only expected to increase the impact force generated on the organoids. The increased impact force generated on the organoids is expected to be illustrated in non-phantom organoid tests.

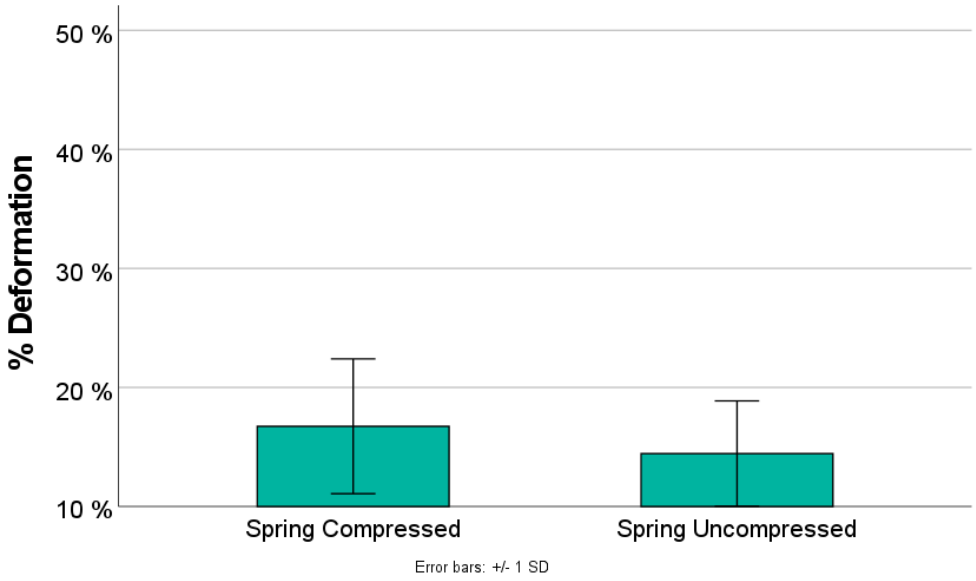


**Figure 4.7:** Spring compression effect over phantom organoid % deformation.

*Sources of Variability*

In each of these tests, there are a number of sources of variability. The first source of variability includes the potential for phantom organoid size to have an effect on deformation. Using the data generated from each of above series of tests, a regression plot, seen in Figure 4.8, illustrates weak correlation between the phantom organoid size and deformation. The data points used included all phantom organoids using the 1 mm stopper height, for consistency, and were differentiated by row in the plot. A histogram describing the frequency of different phantom organoid sizes was also provided. This

result indicates that the size of the phantom organoids does not influence the deformation as there is a weak correlation, and that the stopper height is the main variable affecting deformation.

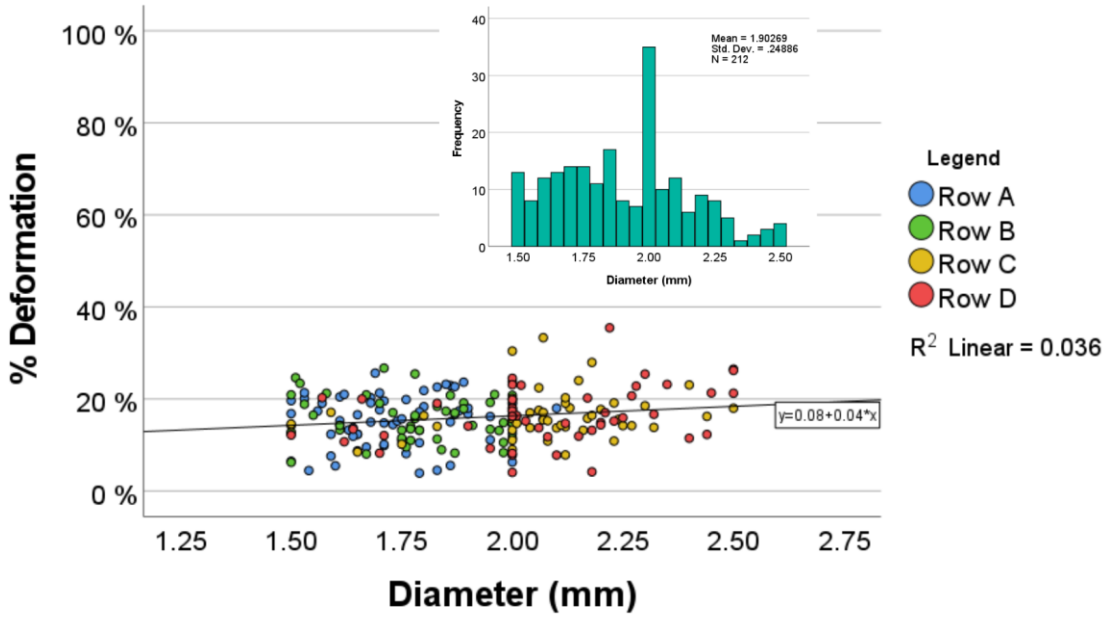


**Figure 4.8:** Correlation between experimental diameter of phantom organoids and experimental % deformation. (Inner) Histogram of frequency of different sized phantom organoids.

In addition, there is expected human error within the measurements of the phantom organoids. To check for error, digital image analysis measuring the exact diameters was performed on a random group of data (sample size of 30 data points), and compared to the measurements made by hand. The measurements made by hand were measured on the short axis of the diameter of the phantom organoids, so the digital measurements did the same. The results of this check showed an approximate 4% ± 0.005% standard error in diameter measurements. The rationale behind using the short axis was that the phantom organoid might not be perfectly spherical, although initially assumed it would be, and that the short axis might better represent the height of the phantom organoid in the well versus the long axis. The low error between digital image measurements to hand measurements provides confidence that these measurements were done correctly.

Furthermore, although the hand versus digital measurements were accurate, there is still potential error that the width of the phantom organoid does not accurately match the height of the phantom organoid in the well. This could be a source of variability because if the phantom organoid is not perfectly spherical, then measuring the width instead of the height will produce incorrect measurements. To check this error, a comparison was performed to measure the difference between measuring width and height. Measuring width was the same as before, but measuring height required a different method. Seen in Figure 4.9, static loading of the organoid at different stopper heights and measuring height changes via digital image analysis was performed. This comparison measured a 3.61% ± 0.007% standard error between height and width measurements, which provides confidence that the phantom organoid can be assumed to be almost perfectly spherical.

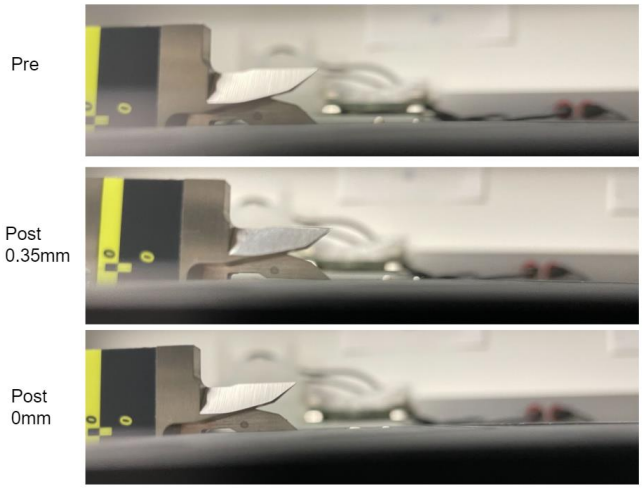


**Figure 4.9:** Static loading error measurements. (Top) Phantom organoids are sitting in their respective wells pre-static loading. (Middle) Phantom organoids are statically loaded at a stopper height of 0.35mm. (Bottom) Phantom organoids are statically loaded at a stopper height of 0mm.

The final source of variability includes potential stopper height human error where the stopper height may not be exactly where it is supposed to be. This might leaded to faulty experimental calculations, and could be a source since theoretical deformation percentages aren't always an exact match with the experimental deformation percentage. Additionally, since the errors above are rather low, error in setting the stopper height to its exact position could be the final potential source. This may be a limitation in the current impactor design, as the stopper height is not known to be exact.

**Brain Organoid Testing**

*Preliminary Trials*

Translating the device from phantom organoids to real organoids was successful although posing its own set of challenges. To effectively ensure that the organoids work with the device, experiments were run to test the limits of the device in combination with the organoids. Initial tests (trial 1), seen in Figure 4.10, where the organoid was placed in row A (depth: 0.75mm, diameter: 2.4mm), successfully injured the organoids and indicated that below a stopper height of 0.2 mm, organoids got completely smashed, stuck to the impact dropper, and were generally unrecoverable. On the other hand, seen in Figure 4.11, organoids at 0.3 mm were damaged, did not stick to the impact dropper, and were recoverable. These results were incredibly promising as it illustrated the success in the impactor device, while also exposing a flaw that the organoids were too small for our organoid holder wells, and that miniscule stopper heights were necessary. With this in mind, an improved organoid holder (Figure 3.8) illustrated in the methods section, was designed to solve this issue. With smaller wells for the organoids, another round of testing ensued to determine the limits of the device in combination with the organoids.

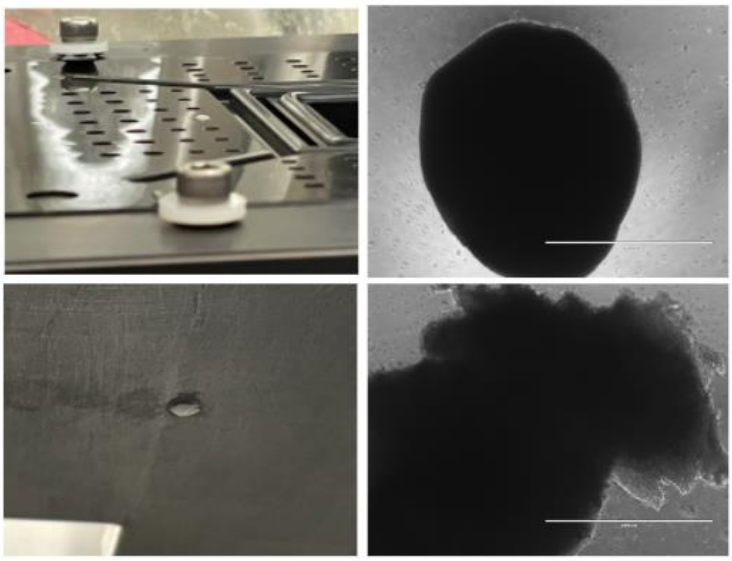

**Figure 4.10:** Trial 1. Old organoid holder, stopper height at 0 mm. (Top-left) Organoid positioning in the well pre-impact. (Bottom-left) Organoid smashed on the bottom surface of the impact dropper post-impact. (Top-right) Imaging of the organoid pre-impact. (Bottom-right) Imaging of the organoid post-impact.

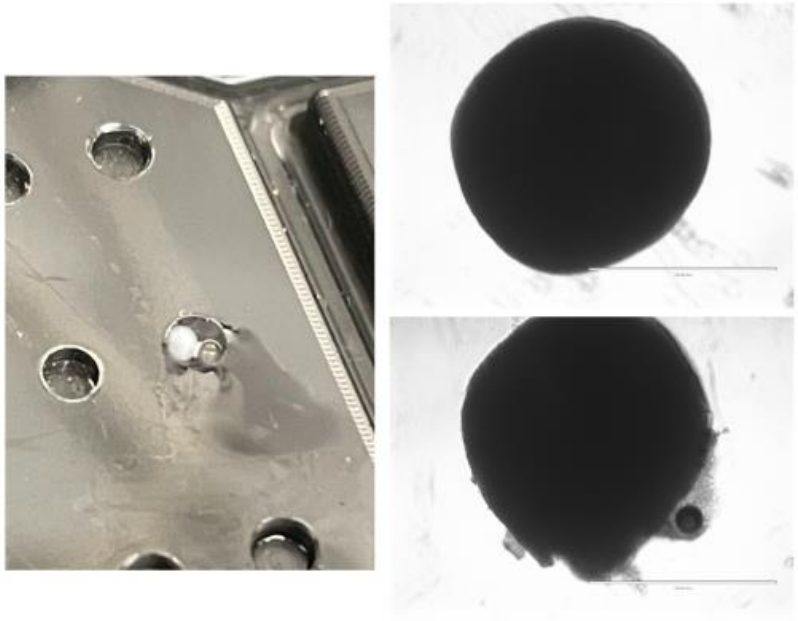

**Figure 4.11**: Trial 1. Old organoid holder, stopper height at 0.3 mm. (Left) Organoid positioning in the well pre-impact. (Top-right) Imaging of the organoid pre-impact. (Bottom-right) Imaging of the organoid post-impact.

Theoretical calculations were made to estimate the deformation induced using the improved organoid holder. Assuming an organoid diameter of 1.2 mm and a well depth of 0.5 mm, by varying the stopper height deformation percentages were calculated, seen in Figure 4.12.

Performing further experiments (trial 2) with row B (depth: 0.5mm, diameter: 2 mm) of the improved organoid holder, organoids were again successfully injured and indicated that at a stopper height at 0.3mm and below, the organoid gets completely smashed and stuck to the bottom surface of the impactor, as seen in Figure 4.13. On the other hand, as seen in Figure 4.14, at a stopper height of 0.4 mm the organoid stayed within the well, were recoverable for imaging, and showed damage. To split the difference, a stopper height of 0.35 mm was tested showing damage without sticking to the impact dropper. It is hypothesized that the organoids may stick to the impact dropper when above an approximate of 30% deformation, based on the results seen. Anything greater than 30% deformation, leads to greater surface area contact, and since the organoids are so light, the surface area that comes into contact may allow for a hydrostatic suction force to lift the organoids out of the well. This stopper height was further

tested with additional spring force. Figure 4.15 illustrates the uncompressed and compressed spring tests at a stopper height of 0.35 mm. These results were very promising as the 0.35 mm test with the spring showed damage to the organoid without sticking to the impact dropper, which demonstrated the potential use for a positive control for future experiments.

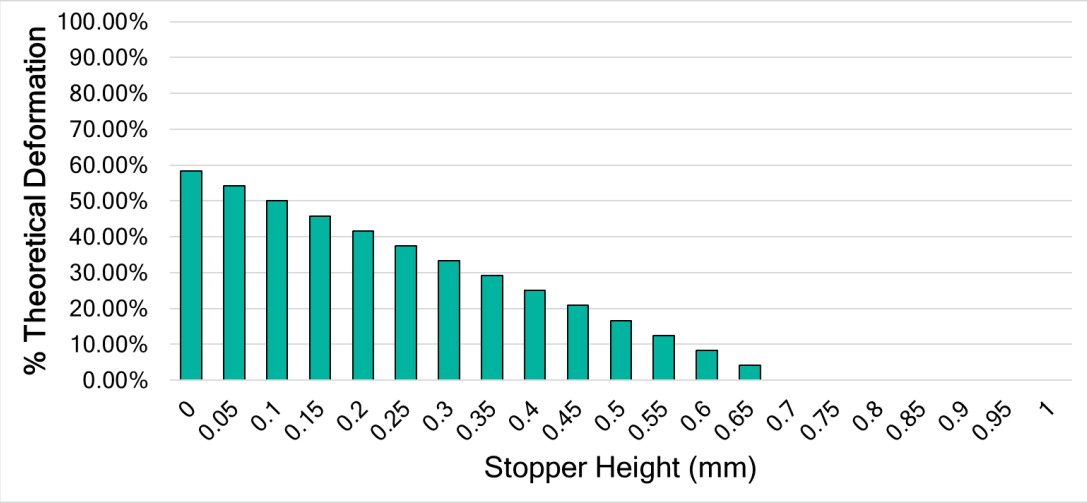


**Figure 4.12:** Theoretical % deformation of real organoids by stopper height using the improved organoid holder.

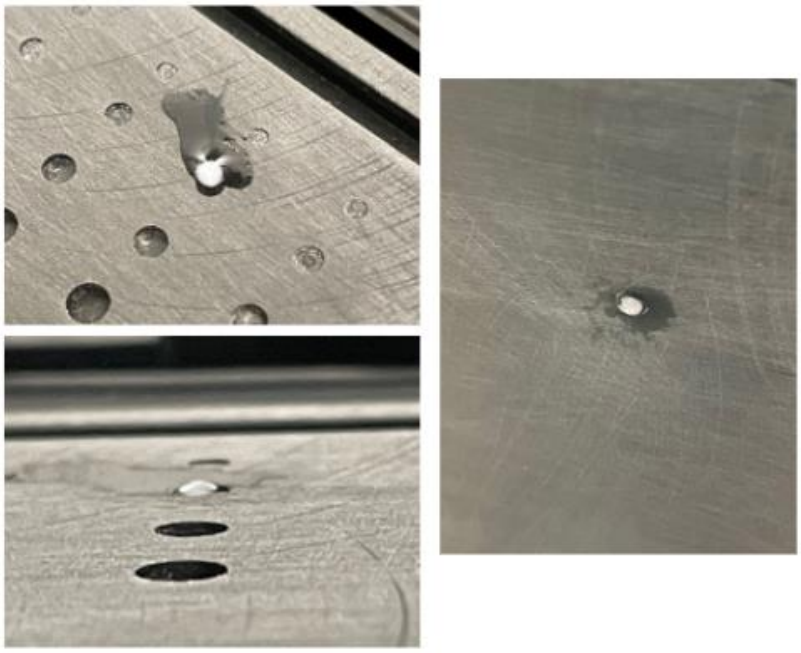

**Figure 4.13:** Trial 2. Improved organoid holder, stopper height at 0 mm. (Top-left) Top-view organoid positioning in the well pre-impact. (Bottom-left) Side-view organoid positioning in the well pre-impact. (Right) Organoid smashed on the bottom surface of the impact dropper post-impact.

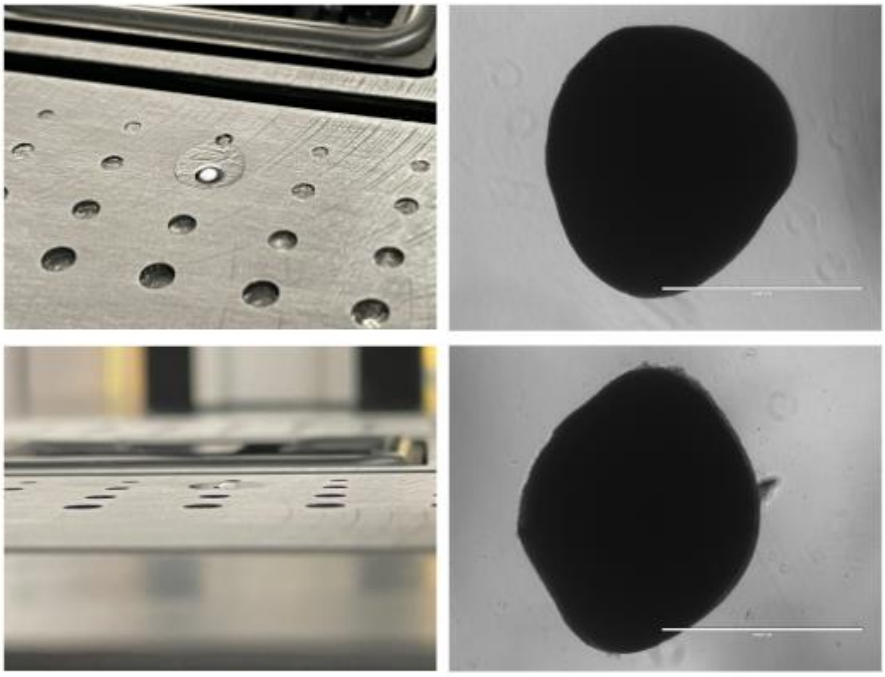

**Figure 4.14:** Trial 2. Improved organoid holder, stopper height at 0.4 mm. (Top-left) Top-view of organoid positioning in the well pre-impact. (Bottom-left) Side-view of the organoid positioning in the well pre-impact. (Top-right) Imaging of the organoid pre-impact. (Bottom-right) Imaging of the organoid post-impact.

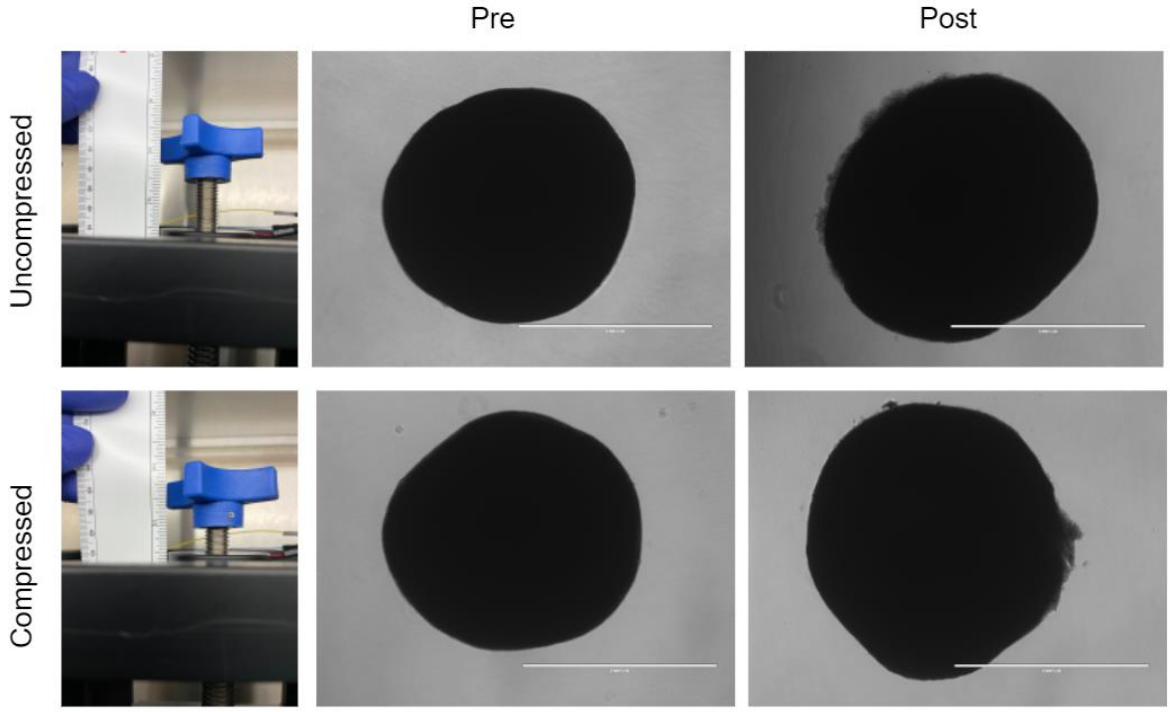


**Figure 4.15:** Trial 2. Improved organoid holder, stopper height at 0.35 mm. (Top) Uncompressed spring images with pre- versus post- impact. (Bottom) Compressed spring images with pre- versus post- impact.

*Positive Control*

The positive control (trial 3) consisted of 6 organoids over 2 tests. The stopper height was set to 0.35 mm, which was determined to be the lowest stopper height without the organoids sticking to the impact dropper, and the spring was compressed 14.04 mm, as it was in the preliminary tests. Figure 4.16 and 4.17 illustrates the damage induced on the organoids from this impact. Damage is fairly variable, since the organoids vary in size and shape, but in each image, there is clear damage either in the total shape or on the surrounding edges of the organoids indicating a successful impact. It is important to note that organoid #3 stuck to the impact dropper, but was recoverable for imaging, and organoid #5 was lost during the transition to post-imaging. The overall structure can be seen as compromised or damaged, but further internal damage will be investigated through IHC staining.

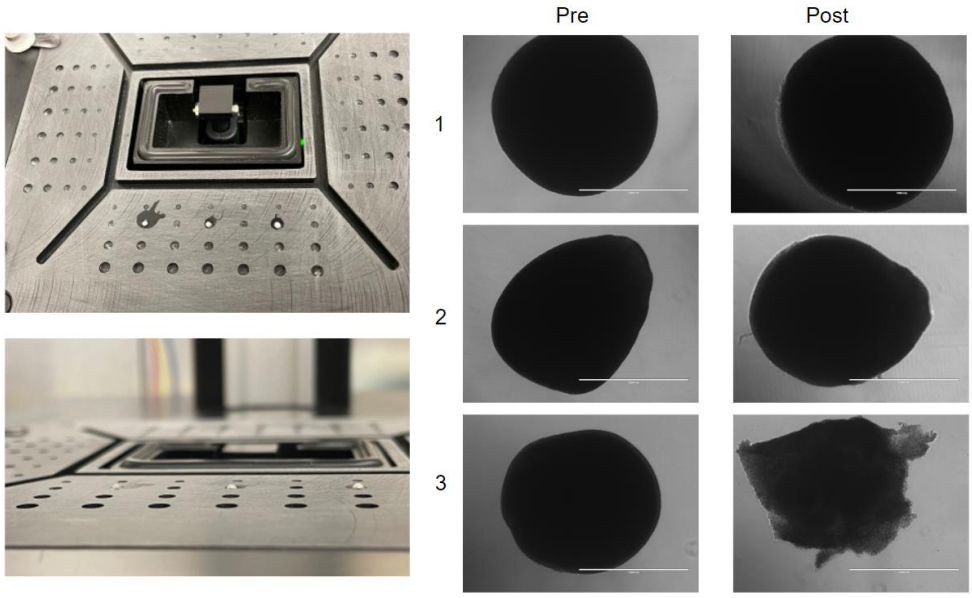


**Figure 4.16:** Trial 3. Positive control, test 1 (organoids 1-3). (Left) Organoid positioning within the organoid holder wells from a top and side view. (Right) Organoid pre- and post- impact imaging for organoids 1-3.

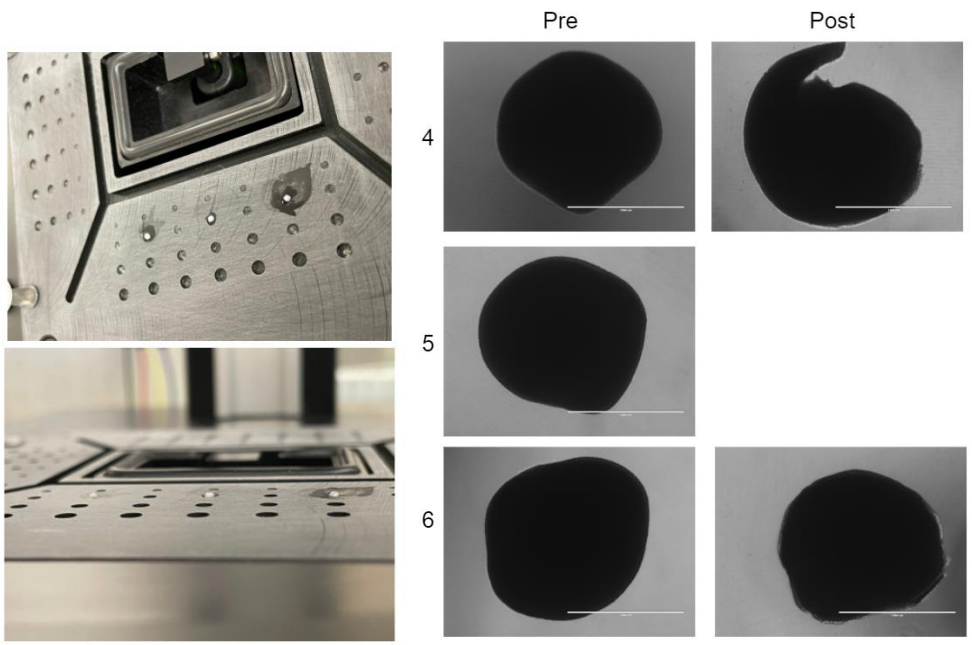


**Figure 4.17:** Trial 3. Positive control, test 2 (organoids 4-6). (Left) Organoid positioning within the organoid holder wells from a top and side view. (Right) Organoid pre- and post- impact imaging for organoids 4-5. Note that organoid #5 was not recoverable, and has no post-impact image.

*Negative Control*

The negative control (trial 3) also consisted of 6 organoids over 2 tests. The stopper height was set to 0.35 mm, and the spring was not compressed. The organoids followed the same protocol of placing and positioning in the organoid holder wells, but there was no impact. Instead, the organoids were placed in the wells for approximately 10 seconds, to conservatively mock the amount of time it takes for a typical impact, and were then removed. Figure 4.18 and 4.19 illustrates the resulting imaging from this experiment. There seems to be none to minimal damage induced to the organoids indicating a successful negative control, but any damage seen to the organoids here may be caused by the pipetting the organoids in and out of the well. It is important to note that organoid #6 required extensive pipetting to remove from the organoid holder well and back into the original dish for imaging. Comparing to the positive control there is a clear difference in damage around the edges of the organoid. The positive control consists of organoids that have strained or damaged edges and broken off pieces, while the negative control at most has a slight strain around the edges of the organoid. Further internal damage will be investigated through IHC staining.

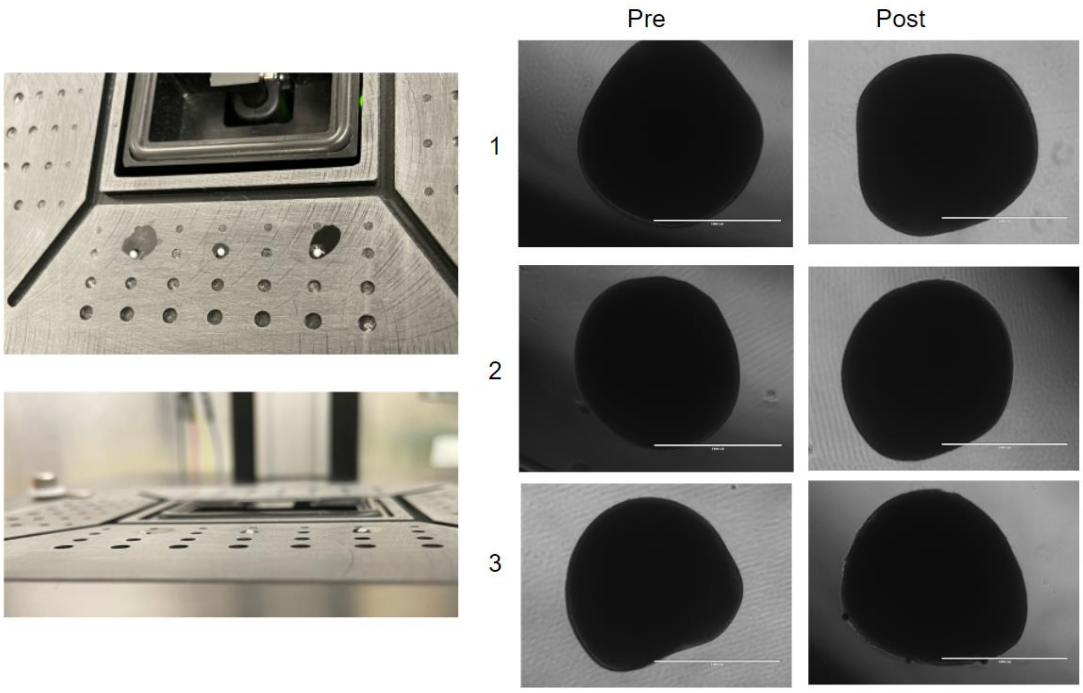


**Figure 4.18:** Trial 3. Negative control, test 1 (organoids 1-3). (Left) Organoid positioning within the organoid holder wells from a top and side view. (Right) Organoid pre- and post- impact imaging for organoids 1-3.

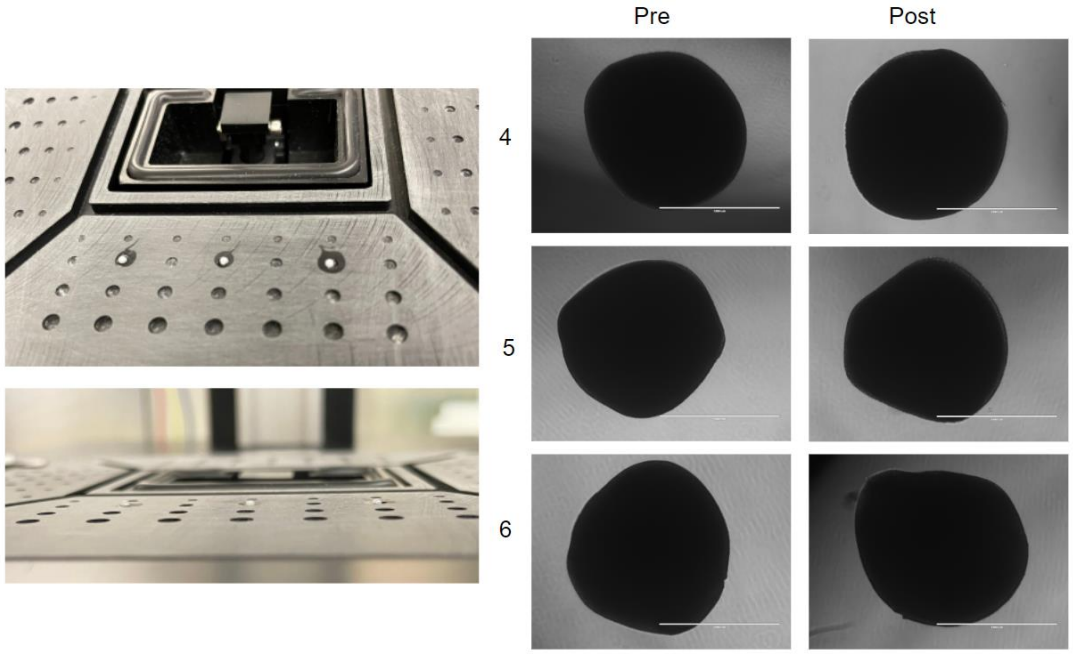


**Figure 4.19:** Trial 3. Negative control, test 2 (organoids 4-6). (Left) Organoid positioning within the organoid holder wells from a top and side view. (Right) Organoid pre- and post- impact imaging for organoids 4-5.

*IHC Staining*

Each trial underwent IHC staining. Trials 1 and 2 were only stained for DAPI, GFAP, and NF200, while trial 3 consisted of DAPI, GFAP, NF200, and Caspase-3. Trial 1, seen in Figure 4.20, corresponds to the tests using the old organoid holder and has a mix of stopper heights consisting of 0mm, 0.2mm, 0.3mm, and 0.5mm. Trial 2, seen in Figure 4.20, corresponds to the tests using the improved organoid holder with a stopper height of 0.4mm.

Both of these trials generated promising results that demonstrated feasibility of the device and the protocol for staining. The images with the NF-200 stain illustrate the general neuronal structure left over after the impact. There are brighter regions around the edge which may indicate that neurons are compressed but not dead. Certain regions where there is no NF-200 staining could be a result of brain organoid pieces breaking off during impact, or error when sectioning the brain organoid leaving small tears. The images with the GFAP stain illustrate glial cell stress and astrocyte activation. Focusing on the brighter red regions is where astrocyte activation may be seen. This is an indication of the post-TBI neuroinflammatory response discussed in the introduction. Most of the astrocyte activation can be seen around the edges, although there is some localized activation in the center of the brain organoid. This may suggest that damage and neuroinflammation in a TBI can be found typically around the edges of the of the brain, but in more severe cases it can penetrate inwards. Damage to the edges could be found from the actual impact, whereas the centrally located damage could be additionally found from internal pressurized fluid movement that induces more stress.

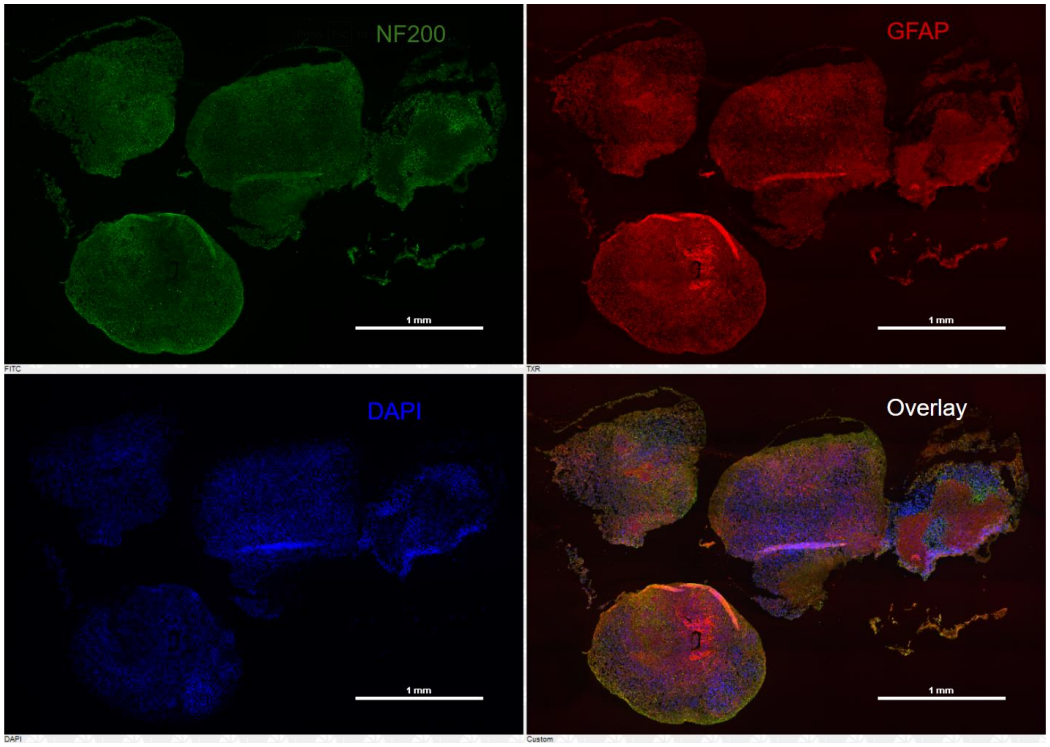


**Figure 4.20:** Trial 1, IHC Staining. Old organoid holder with varying stopper heights. Stains: (green) NF-200, (red) GFAP, (blue) DAPI. Scale at 1mm.

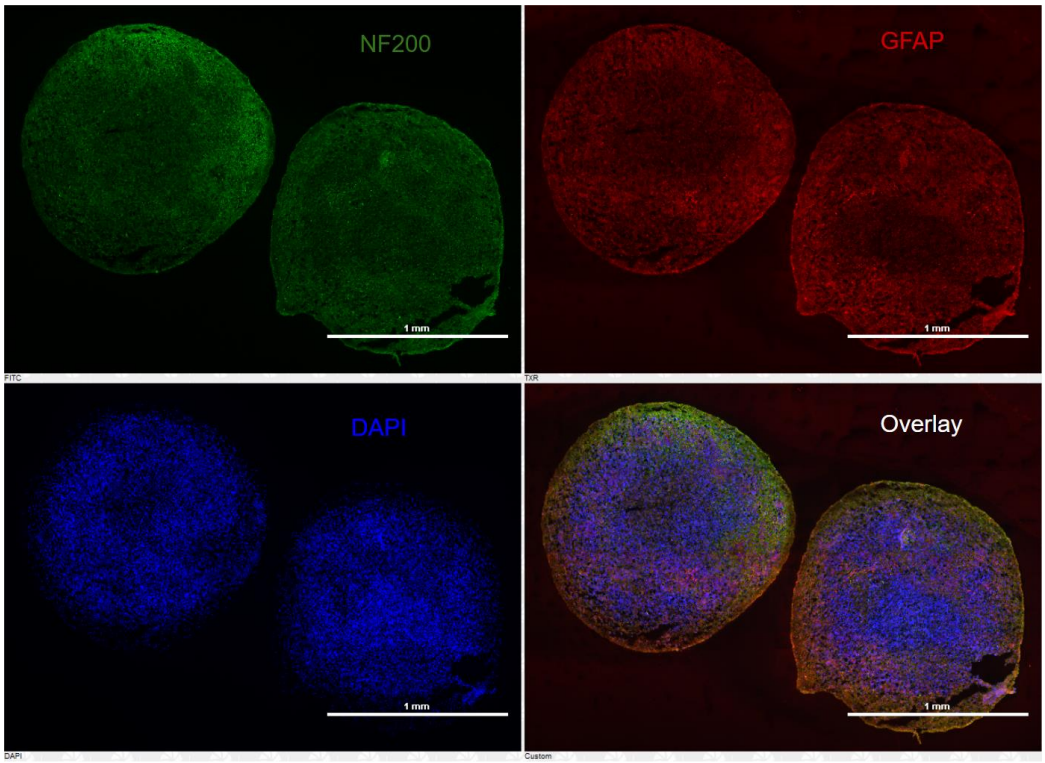


**Figure 4.21:** Trial 2, IHC Staining. Improved organoid holder at stopper height of 0.4mm. Stains: (green) NF-200, (red) GFAP, (blue) DAPI. Scale at 1mm.

Although staining and imaging was successful, the protocol needed to be troubleshooted as the GFAP fluorescent stains came off much stronger than anticipated. For trial 3, a new GFAP antibody was used, in addition to a Caspase-3 stain. Trial 3, seen in Figures 4.22 and 4.23, corresponds to the positive and negative controls. The positive control consists of an impact with a stopper height of 0.35mm and additional spring force that generates a calculated force of 20N. In Figure 4.22, a specific region is focused on to provide insight into the general response. NF-200 signal is produced all around, but in this region, there are portions with limited to none signal, that may indicate neurons no longer exist or are suppressed in these regions. Interestingly, the DAPI signal illustrates a circular structure that resembles a rosette formation, which may be an antibody-forming cell. More importantly, GFAP and Caspase-3 stains provide significant results as damage indicators. GFAP marks neuroinflammation as a result of astrocyte activation, and Caspase-3 marks neuronal apoptosis as a result of increased caspase proteases. The bright red signals in the GFAP stain illustrate the neuroinflammation induced as a result of impact and secondary injury. Similarly, the bright green signals in the Caspase-3 stain illustrate neuronal apoptosis as a result of impact and secondary injury.

In contrast, Figure 4.23 consists of the negative control with no impact under the same conditions as the positive control. Focusing on only the GFAP and Caspase-3 stains, the negative control indicates significantly less damage, neuroinflammation, and apoptosis. There is some GFAP signal which may be caused by pipetting the organoid in and out of the device, which is consistent with previous negative controls. There is little to none signaling of Caspase-3 indicating that neuronal cells are not dying.

These control experiments suggest that IHC allows the experimenter to evaluate markers of astrocyte activation through GFAP, and apoptotic pathways through Caspase-3. As expected, positive controls of approximately 30% deformation resulted in substantial GFAP and Caspase-3 expression. These results are significant because they indicate that the impact device was successful in inducing a TBI response in these brain organoids, the main goal of this thesis.

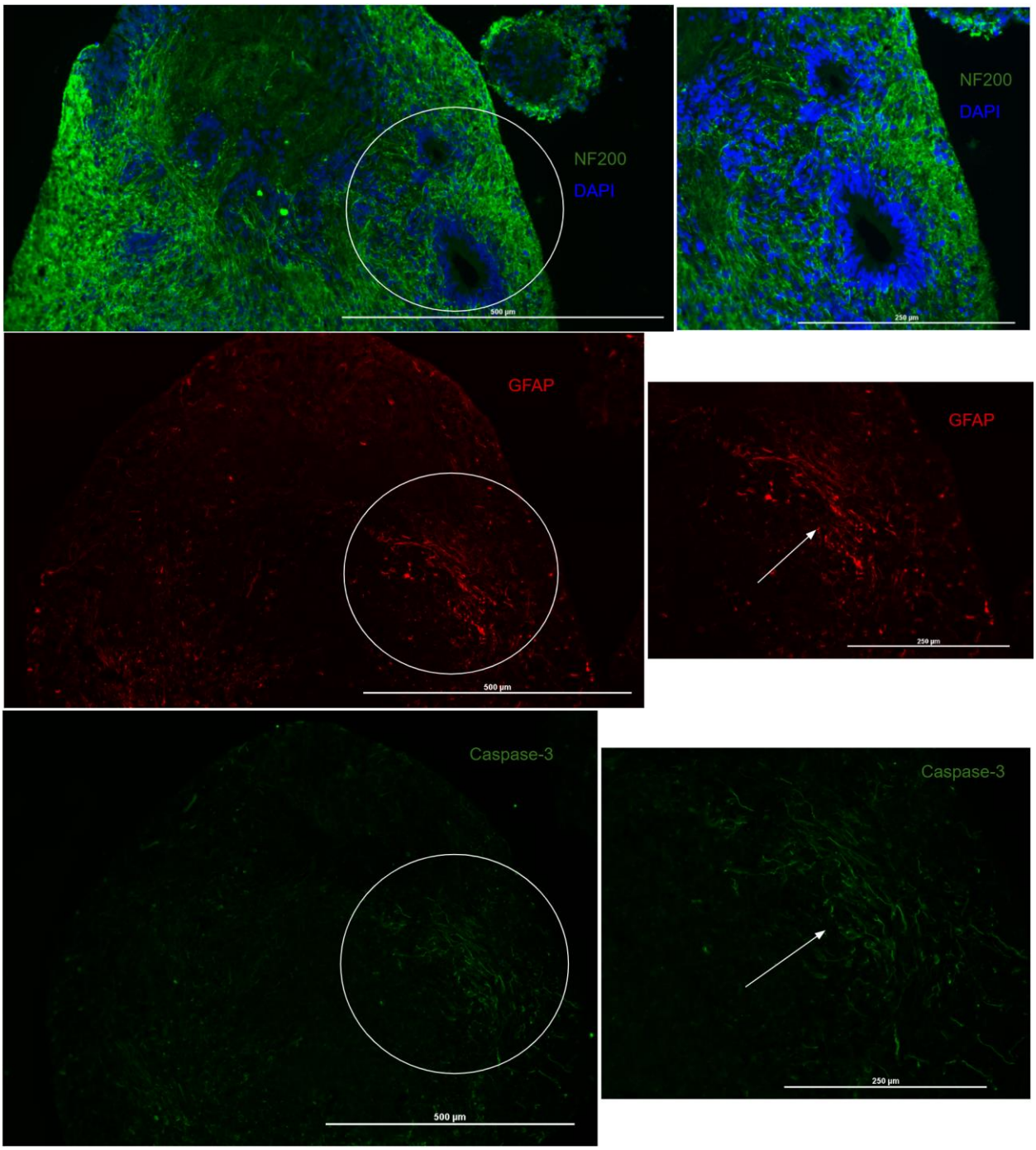


**Figure 4.22:** Trial 3, Positive Control - IHC Staining. Improved organoid holder at stopper height of 0.35mm with additional spring force. (Top) NF-200 (green) and DAPI (blue) staining with zoomed in image on a point of interest. (Middle) GFAP (red) staining with zoomed in image on a point of interest. (Bottom) Caspase-3 (green) staining with zoomed in image on a point of interest. Overall scale at 500 microns and zoomed in scale at 250 microns.

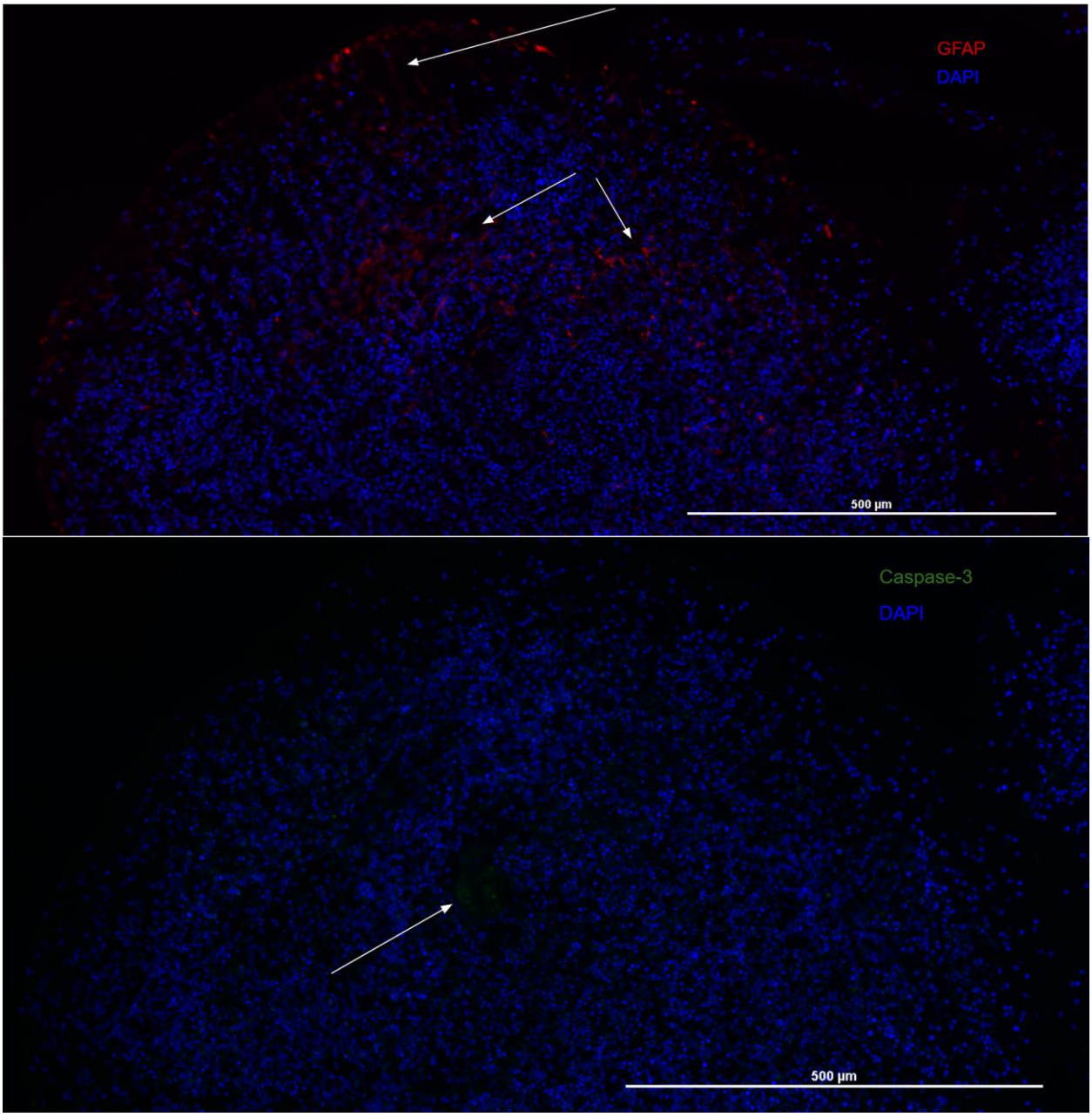


**Figure 4.23:** Trial 3, Negative Control - IHC Staining. Improved organoid holder at stopper height of 0.35mm with no impact. (Top) GFAP (red) and DAPI (blue) staining. (Bottom) Caspase-3 (green) and DAPI (blue) staining. Scale at 500 microns.

Despite these significant results, there were some limitations with the model and IHC protocol. Critical information on the orientation and tracking of specific organoids is missing. When transferring from post-injury to cryo-freezing each of the organoids were placed together based on their testing group. In addition, the organoids are not specifically oriented in such a way to be perpendicular to the axis of deformation. With this in mind, these organoids then become much more difficult to track and compare between IHC imaging and EVOS imaging. With more time and more careful placement, by placing one organoid per cryo-frozen block and delicately orienting it in such a manner to could ensure approximate placement perpendicular to the axis of deformation and tracking of each specific organoid.

Another limitation includes the difficulty of pipetting the organoids in and out of the organoid holder well. Since the organoids and the wells are quite small, the pipette tip does not easily suck the organoids out, as it sometimes took multiple tries and the addition of more media to remove the organoid from the well. This difficulty may have induced additional damage to the organoids which may be seen in the negative control experiments (Figure 4.23). A solution to pipetting difficulty would be beneficial in improving the overall quality and efficiency of the experiment, which could include a new organoid holder designed for pipetting ease. Additionally, visually placing the organoids required magnification using an iPhone-12 camera, which worked well. This may not be available or efficient for each experiment as you would need two users to run the experiement, so a solution could include a magnifying glass attached to the device.

The last limitation comments on the accuracy of the biomechanical injury of the impact device in comparison to the biomechanical injury of a real-life TBI. The current injury model for this device looks at organoid tissue being impacted directly, when in reality there is a skull-like barrier that protects the brain. The actual injury that occurs in TBI is when the brain bounces and impacts the internal wall of the skull after external impact. With this in mind, future iterations of this device could include a modified impact dropper that has skull-like barrier with a hollow interior to place organoids and their relative media within. This potentially could more accurately model the biomechanics of a real-life TBI.

# CONCLUSION

In this study, we were challenged to help provide a greater understanding of TBI and improve translation between preclinical and clinical models. More specifically, the main aim was to design and develop a device, simpler than its predecessors, to accurately and efficiently injure brain organoids. Throughout this thesis, the rationale behind this design was listed demonstrating the requirements and the iterative process toward the final design, the mechanisms and protocol for the device was explained to illustrate how the design meets the original requirements, the accuracy and efficacy of the device was tested through the use of phantom organoid conveying that this device worked as designed, and the application to TBI through the use of human organoids provided pivotal evidence that this device can be utilized in a multitude and variety of experiments for TBI research.

This human organoid impactor device meets all of its requirements laid out at the beginning of design. The device is compact and portable, as it fits within the standard lab hood, and is easily transportable for a variety of experiments. The device is also easy to manufacture, assemble, and use, as the mechanisms of the device are very simple, easy to explain, and only require minimal preparation time. In addition, this device allows for easy deconstruction and replacement of parts, in case any changes must be made. For example, the organoid holder can be changed and replaced as long as it fits within the slot, the post can be replaced with a shorter post for lower velocity tests, and the spring can be easily replaced for varying forces. The design only cost about $900, without manufacturing costs. The device was easily sterilizable as it was cleaned with ethanol and the parts that would touch the organoids could undergo UV light sterilization. Most importantly, the device allowed for efficient and variable experimental use. The device has significantly increased the production output of injured brain organoids in a short amount of experimental time, and the device allows for the ability to induce different levels of severity through the control of deformation of the organoid and the force and velocity of the impact placed upon the organoids. The device also allows for variability in the organoid holder since there are multiple sized

wells for different sized organoids or applications. As stated before, the organoid holder can be easily replaced as well for further variability.

Improvements that could be made to this device include an even more compact design, a design that includes two opposing guide rails so that the impact dropper falls more evenly, more compatible organoid holders for easy pipetting, a magnifying glass to make the organoids more visible to the user, and a better battery source since the battery needs to be replaced a lot. Improvements to the testing model include better measurements of the actual height of the organoid versus the actual deformation, real velocity and force measurements instead of just calculated velocity and force, more confident stopper height control, a better solution to the organoids sticking to the impact dropper, an optimized experimental IHC protocol with clear tracking and orientation of the organoids pre-injury to post-injury to IHC stain imaging, and a new skull-like impact design to model real-life TBI conditions of a brain within the skull. Additionally, studies determining relationships between velocity, force, and deformation of a TBI on human brains could be beneficial in future experiments with the current design and also with a skull-like impact design.

Overall, this thesis provides a significant step forward from previous organoid injury models for TBI research. The organoid impactor device shows potential to accurately injure organoids by varying deformation and forces, and through further iterations and improvement, the device can easily prove to be a pivotal tool to greater understand TBI and improve translation between preclinical and clinical models.

APPENDIX

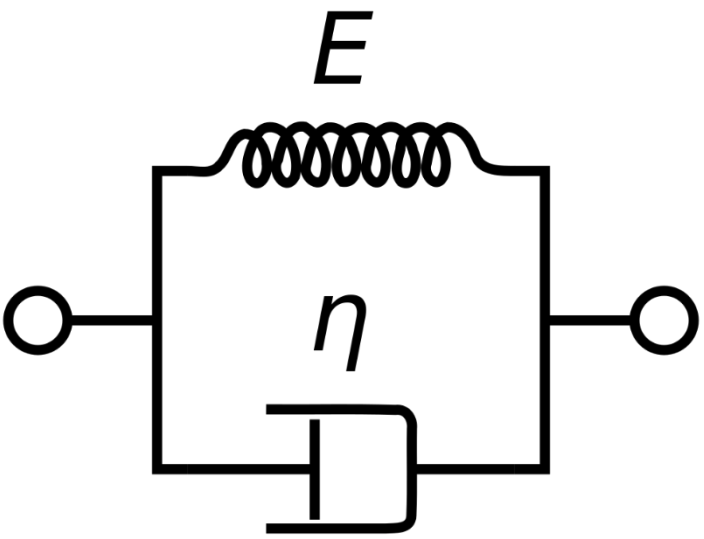


Appendix 1: Kelvin-Voigt Viscoelastic Model Schematic.

```
%Force Velocity Analysis
%Conversions
g = 9.81; %m/s^2
in2mm = 25.4; %mm
lb2g = 453.592; %g
lbin2Nmm = 0.175; %N/mm

%Variables

mplate = 273; %g
kspring = 7 * lbin2Nmm;
l_c = (0:0.01:1.34) * in2mm; %Max 1.34
distance = 17.8*in2mm; %Max 15

F = (mplate/1000 * g) + ((kspring) * l_c);
v = sqrt((2*F*distance/1000)/(mplate/1000));

subplot(2,2,1)
plot(l_c, v)
xlabel('Compression of Spring (mm)')
ylabel('Velocity (m/s)')

subplot(2,2,2)
plot(l_c, F)
xlabel('Compression of Spring (mm)')
ylabel('Force (N)')


for k = 1:1:10
    F = (mplate * g / 1000) + ((k) * lbin2Nmm * l_c);
    v = sqrt((2*F*distance/1000)/(mplate/1000));

    subplot(2,2,4);
    plot(l_c,F)
    hold on
    xlabel('Compression of Spring (mm)')
    ylabel('Force (N)')



    subplot(2,2,3);
    plot(l_c,v)
    hold on
    xlabel('Compression of Spring (mm)')
    ylabel('Velocity (m/s)')

end

hold off
```

Appendix 2: MATLAB Force-Velocity Analysis.

```
#include <Wire.h>
#include "Adafruit_VL53L0X.h"
#include <Servo.h>

Servo actuator;

const int ACTUATOR_PIN = 1;
bool isOpen = false;
Adafruit_VL53L0X rangeSensor = Adafruit_VL53L0X();

void setup() {
  // wait for range sensor to start
  if (! rangeSensor.begin()) {
    while (1);
  }

  actuator.attach(ACTUATOR_PIN); //Connects the actuator code to the actuator pin where information is sent to the arduino
}

void closeActuator(bool doDelay = true) {
  actuator.writeMicroseconds(1777); //Height at which the actuator is closed at. Fully closed is at 2000. Reference actuator
                                    //stopper height code for value depending on stopper height.
  if (doDelay) {
    delay(3000); //delay so that full action is completed before next action
  }
}



void openActuator(bool doDelay = true) {
  actuator.writeMicroseconds(1000); //Height at which the actuator is open at. Fully open is at 1000.
  if (doDelay) {
    delay(3000); //delay so that full action is completed before next action
  }
}

void loop() {
 VL53L0X_RangingMeasurementData_t measure;
 rangeSensor.rangingTest(&measure, false); // pass in 'true' to get debug data printout!

  // if we have no errors and range is low, we close, otherwise open.
  if (measure.RangeStatus != 4 && measure.RangeMilliMeter < 110) { //Distance (mm) between the sensor and the impact dropper
                                                                   //at which the signal is sent to the actuator (max is 1000)
    closeActuator(isOpen); //if the distance is <value then the actuator stays closed
    isOpen = false;
  } else if (!isOpen) { //if the distance is not <value then the actuator opens
    openActuator();
    isOpen = true;
  }

  delay(50);
}
```

Appendix 3: TOF & Actuator Calibration Code.

REFERENCES

[1] Agoston, D. V., Shutes-David, A., & Peskind, E. R. (2017). Biofluid biomarkers of traumatic brain injury. *Brain injury*, 31(9), 1195–1203. https://doi.org/10.1080/02699052.2017.1357836

[2] Akamatsu, Y., & Hanafy, K. A. (2020). Cell Death and Recovery in Traumatic Brain Injury. *Neurotherapeutics : the journal of the American Society for Experimental NeuroTherapeutics*, 17(2), 446–456. https://doi.org/10.1007/s13311-020-00840-7

[3] Burda, J. E., Bernstein, A. M., & Sofroniew, M. V. (2016). Astrocyte roles in traumatic brain injury. *Experimental neurology*, 275 Pt 3(0 3), 305–315. https://doi.org/10.1016/j.expneurol.2015.03.020

[4] Capizzi, A., Woo, J., & Verduzco-Gutierrez, M. (2020). Traumatic Brain Injury: An Overview of Epidemiology, Pathophysiology, and Medical Management. *The Medical clinics of North America*, 104(2), 213–238. https://doi.org/10.1016/j.mcna.2019.11.001

[5] Cash, A., & Theus, M. H. (2020). Mechanisms of Blood-Brain Barrier Dysfunction in Traumatic Brain Injury. *International journal of molecular sciences*, 21(9), 3344. https://doi.org/10.3390/ijms21093344

[6] Centers for Disease Control and Prevention. (2022). TBI Data. *Traumatic Brain Injury & Concussion*. https://www.cdc.gov/traumaticbraininjury/data/index.html

[7] Chen, H. I., Song, H., & Ming, G. L. (2019). Applications of Human Brain Organoids to Clinical Problems. *Developmental dynamics : an official publication of the American Association of Anatomists*, 248(1), 53–64. https://doi.org/10.1002/dvdy.24662

[8] Chen, Y., Mao, H., Yang, K. H., Abel, T., & Meaney, D. F. (2014). A modified controlled cortical impact technique to model mild traumatic brain injury mechanics in mice. *Frontiers in neurology*, 5, 100. https://doi.org/10.3389/fneur.2014.00100

[9] Chiu, C. C., Liao, Y. E., Yang, L. Y., Wang, J. Y., Tweedie, D., Karnati, H. K., Greig, N. H., & Wang, J. Y. (2016). Neuroinflammation in animal models of traumatic brain injury. *Journal of neuroscience methods*, 272, 38–49. https://doi.org/10.1016/j.jneumeth.2016.06.018

[10] Chudler, E. (2022). Brain Facts and Figures. *University of Washington.* https://faculty.washington.edu/chudler/facts.html

[11] Donat, C. K., Yanez Lopez, M., Sastre, M., Baxan, N., Goldfinger, M., Seeamber, R., Müller, F., Davies, P., Hellyer, P., Siegkas, P., Gentleman, S., Sharp, D. J., & Ghajari, M. (2021). From biomechanics to pathology: predicting axonal injury from patterns of strain after traumatic brain injury. *Brain : a journal of neurology*, 144(1), 70–91. https://doi.org/10.1093/brain/awaa336

[12] Fischer, J., Heide, M., & Huttner, W. B. (2019). Genetic Modification of Brain Organoids. *Frontiers in cellular neuroscience*, 13, 558. https://doi.org/10.3389/fncel.2019.00558

[13] Fung, Y.C. (1993). *Biomechanics: Mechanical Properties of Living Tissues*. Springer New York. https://doi.org/10.1007/978-1-4757-2257-4

[14] Graham, N. S., & Sharp, D. J. (2019). Understanding neurodegeneration after traumatic brain injury: from mechanisms to clinical trials in dementia. *Journal of neurology, neurosurgery, and psychiatry*, 90(11), 1221–1233. https://doi.org/10.1136/jnnp-2017-317557

[15] Hier, D. B., Obafemi-Ajayi, T., Thimgan, M. S., Olbricht, G. R., Azizi, S., Allen, B., Hadi, B. A., & Wunsch, D. C., 2nd (2021). Blood biomarkers for mild traumatic brain injury: a selective review of unresolved issues. *Biomarker research*, 9(1), 70. https://doi.org/10.1186/s40364-021-00325-5

[16] Hodge, R. D., Bakken, T. E., Miller, J. A., Smith, K. A., Barkan, E. R., Graybuck, L. T., Close, J. L., Long, B., Johansen, N., Penn, O., Yao, Z., Eggermont, J., Höllt, T., Levi, B. P., Shehata, S. I., Aevermann, B., Beller, A., Bertagnolli, D., Brouner, K., Casper, T., … Lein, E. S. (2019). Conserved cell types with divergent features in human versus mouse cortex. *Nature*, 573(7772), 61–68. https://doi.org/10.1038/s41586-019-1506-7

[17] Hsieh, T. H., Kang, J. W., Lai, J. H., Huang, Y. Z., Rotenberg, A., Chen, K. Y., Wang, J. Y., Chan, S. Y., Chen, S. C., Chiang, Y. H., & Peng, C. W. (2017). Relationship of mechanical impact magnitude to neurologic dysfunction severity in a rat traumatic brain injury model. *PloS one*, 12(5), e0178186. https://doi.org/10.1371/journal.pone.0178186

[18] Keating, C. E., & Cullen, D. K. (2021). Mechanosensation in traumatic brain injury. *Neurobiology of disease*, 148, 105210. https://doi.org/10.1016/j.nbd.2020.105210

[19] Lacalle-Aurioles, M., Cassel de Camps, C., Zorca, C. E., Beitel, L. K., & Durcan, T. M. (2020). Applying hiPSCs and Biomaterials Towards an Understanding and Treatment of Traumatic Brain Injury. *Frontiers in cellular neuroscience*, 14, 594304. https://doi.org/10.3389/fncel.2020.594304

[20] Magliaro, C., Rinaldo, A., & Ahluwalia, A. (2019). Allometric Scaling of physiologically-relevant organoids. *Scientific reports*, 9(1), 11890. https://doi.org/10.1038/s41598-019-48347-2

[21] Marklund N. (2016). Rodent Models of Traumatic Brain Injury: Methods and Challenges. *Methods in molecular biology* (Clifton, N.J.), 1462, 29–46. https://doi.org/10.1007/978-1-4939-3816-2_3

[22] Najem, D., Rennie, K., Ribecco-Lutkiewicz, M., Ly, D., Haukenfrers, J., Liu, Q., Nzau, M., Fraser, D. D., & Bani-Yaghoub, M. (2018). Traumatic brain injury: classification, models, and markers. *Biochemistry and cell biology*, 96(4), 391–406. https://doi.org/10.1139/bcb-2016-0160

[23] Nzou, G., Wicks, R. T., VanOstrand, N. R., Mekky, G. A., Seale, S. A., El-Taibany, A., Wicks, E. E., Nechtman, C. M., Marrotte, E. J., Makani, V. S., Murphy, S. V., Seeds, M. C., Jackson, J. D., & Atala, A. J. (2020). Author Correction: Multicellular 3D Neurovascular Unit Model for Assessing Hypoxia and Neuroinflammation Induced Blood-Brain Barrier Dysfunction. *Scientific reports*, 10(1), 20384. https://doi.org/10.1038/s41598-020-77348-9

[24] O'Brien, W. T., Pham, L., Symons, G. F., Monif, M., Shultz, S. R., & McDonald, S. J. (2020). The NLRP3 inflammasome in traumatic brain injury: potential as a biomarker and therapeutic target. *Journal of neuroinflammation*, 17(1), 104. https://doi.org/10.1186/s12974-020-01778-5

[25] Oyefeso, F. A., Muotri, A. R., Wilson, C. G., & Pecaut, M. J. (2021). Brain organoids: A promising model to assess oxidative stress-induced central nervous system damage. *Developmental neurobiology*, 81(5), 653–670. https://doi.org/10.1002/dneu.22828

[26] Pearn, M. L., Niesman, I. R., Egawa, J., Sawada, A., Almenar-Queralt, A., Shah, S. B., Duckworth, J. L., & Head, B. P. (2017). Pathophysiology Associated with Traumatic Brain Injury: Current Treatments and Potential Novel Therapeutics. *Cellular and molecular neurobiology*, 37(4), 571–585. https://doi.org/10.1007/s10571-016-0400-1

[27] Semple, B. D., Blomgren, K., Gimlin, K., Ferriero, D. M., & Noble-Haeusslein, L. J. (2013). Brain development in rodents and humans: Identifying benchmarks of maturation and vulnerability to injury across species. *Progress in neurobiology, 106-107*, 1–16. https://doi.org/10.1016/j.pneurobio.2013.04.001

[28] Shi, W., Dong, P., Kuss, M. A., Gu, L., Kievit, F., Kim, H. J., & Duan, B. (2021). Design and Evaluation of an In Vitro Mild Traumatic Brain Injury Modeling System Using 3D Printed Mini Impact Device on the 3D Cultured Human iPSC Derived Neural Progenitor Cells. *Advanced healthcare materials*, 10(12), e2100180. https://doi.org/10.1002/adhm.202100180

[29] Sussman, E. S., Pendharkar, A. V., Ho, A. L., & Ghajar, J. (2018). Mild traumatic brain injury and concussion: terminology and classification. *Handbook of clinical neurology*, 158, 21–24. https://doi.org/10.1016/B978-0-444-63954-7.00003-3

[30] Tan, H. Y., Cho, H., & Lee, L. P. (2021). Human mini-brain models. *Nature biomedical engineering*, 5(1), 11–25. https://doi.org/10.1038/s41551-020-00643-3

[31] Toman, E., Harrisson, S., & Belli, T. (2016). Biomarkers in traumatic brain injury: a review. *Journal of the Royal Army Medical Corps*, 162(2), 103–108. https://doi.org/10.1136/jramc-2015-000517

[32] Tomar, G. S., Singh, G. P., Lahkar, D., Sengar, K., Nigam, R., Mohan, M., & Anindya, R. (2018). New biomarkers in brain trauma. *Clinica chimica acta; international journal of clinical chemistry*, 487, 325–329. https://doi.org/10.1016/j.cca.2018.10.025

[33] Trauma Victoria. (2021). Traumatic Brain Injury. *Trauma System Guidelines*. https://trauma.reach.vic.gov.au/guidelines/traumatic-brain-injury/introduction

[34] Trujillo, C. A., & Muotri, A. R. (2018). Brain Organoids and the Study of Neurodevelopment. *Trends in molecular medicine*, 24(12), 982–990. https://doi.org/10.1016/j.molmed.2018.09.005

[35] Wang, K. K., Yang, Z., Zhu, T., Shi, Y., Rubenstein, R., Tyndall, J. A., & Manley, G. T. (2018). An update on diagnostic and prognostic biomarkers for traumatic brain injury. *Expert review of molecular diagnostics*, 18(2), 165–180. https://doi.org/10.1080/14737159.2018.1428089

[36] Wang, H., Zhu, X., Liao, Z., Xiang, H., Ren, M., Xu, M., & Zhao, H. (2018). Novel-graded traumatic brain injury model in rats induced by closed head impacts. *Neuropathology: official journal of the Japanese Society of Neuropathology*, 38(5), 484–492. https://doi.org/10.1111/neup.12509

[37] Wu, Y. H., Rosset, S., Lee, T. R., Dragunow, M., Park, T., & Shim, V. (2021). In Vitro Models of Traumatic Brain Injury: A Systematic Review. *Journal of neurotrauma*, 38(17), 2336–2372. https://doi.org/10.1089/neu.2020.7402

[38] Zhang, W., Capilnasiu, A., & Nordsletten, D. (2021). Comparative Analysis of Nonlinear Viscoelastic Models Across Common Biomechanical Experiments. *Journal of Elasticity*, 145(1-2), 117-152. https://doi.org/10.1007/s10659-021-09827-7